

GRID-CONNECTED IN-STREAM HYDROELECTRIC GENERATION BASED ON
THE DOUBLY FED INDUCTION MACHINE

A Thesis

Presented in Partial Fulfillment of the Requirements for the

Degree of Master of Science

with a

Major in Electrical Engineering

in the

College of Graduate Studies

University of Idaho

by

Timothy J. Lenberg

July 2014

Major Professor: Herbert L. Hess, Ph.D.

AUTHORIZATION TO SUBMIT THESIS

This thesis by Timothy J. Lenberg, submitted for the degree of Master of Science with a Major of Electrical Engineering and titled "Grid-Connected In-Stream Hydroelectric Generation Based on the Doubly Fed Induction Machine," has been reviewed in final form. Permission, as indicated by the signatures and dates below, is now granted to submit final copies to the College of Graduate Studies for approval.

Major Professor: _____ Date: _____
Herbert L. Hess, Ph.D.

Committee
Members: _____ Date: _____
Brian K. Johnson, Ph.D.

Tao Xing, Ph.D.

Department
Administrator: _____ Date: _____
Fred Barlow, Ph.D.

Discipline's
College Dean: _____ Date: _____
Larry Stauffer, Ph.D.

Final Approval and Acceptance

Dean of the College
of Graduate Studies: _____ Date: _____
Jie Chen, Ph.D.

ABSTRACT

Within the United States, there is a growing demand for new environmentally friendly power generation. This has led to a surge in wind turbine development. Unfortunately, wind is not a stable prime mover, but water is. Why not apply the advances made for wind to in-stream hydroelectric generation? One important advancement is the creation of the Doubly Fed Induction Machine (DFIM). This thesis covers the application of a gearless DFIM topology for hydrokinetic generation. After providing background, this thesis presents many of the options available for the mechanical portion of the design. A mechanical turbine is then specified. Next, a method is presented for designing a DFIM including the actual design for this application. In Chapter 4, a simulation model of the system is presented, complete with a control system that maximizes power generation based on water speed. This section then goes on to present simulation results demonstrating proper operation.

ACKNOWLEDGEMENTS

All of the power professors at the University of Idaho were instrumental in my continuing education. The most important professor to acknowledge would be my major professor, Dr. Herbert L. Hess. He has been my friend and mentor throughout graduate school. He is the person who made graduate school a possibility by helping me find funding. He has been an incredible sounding board throughout my research and is always there to talk out my latest idea. He is extremely knowledgeable in his field, but he is not ashamed to let you know when he does not have the answer and will work with you to determine what it might be. He is always willing to learn new things, even when they come from people with less experience or degrees than him. Another professor who deserves acknowledgement is Dr. Joseph D. Law. When I came to the university, I knew that I wanted to be an electrical engineer, but I did not know what exactly I wanted to do. It was Dr. Law's teaching and guidance that made me realize that my future was in the power industry and that my passion was electric machinery. Last but not least, I want to acknowledge Dr. Brian K. Johnson. He is a great professor and is greatly missed as department chair. He has been willing to help me work things out every step of the way and helped me realize that, although my first love is machines, I am gifted in all areas related to the power industry.

I want to acknowledge the contributions from the Department of Electrical and Computer Engineering. They gave me the chance to come and learn things I never imagined. It was the Electrical and Computer Engineering Graduate Fellowship I received from them that paid for my first year of graduate school. Without it, I would not have continued.

My final acknowledgement is to Schweitzer Engineering Laboratories (SEL). SEL has provided me employment three different times during my undergraduate and graduate degrees. I was employed two summers during my undergraduate degree in their Engineering Services Division where I learned a lot about automation in the power industry. These internships allowed me to pay for the remainder of my undergraduate tuition. In addition, Normann Fischer lobbied to bring me back on as Interim Support in Research and Development when my graduate fellowship ended. Normann saw my value and potential and was willing to fight in order to have me on his team. It was this employment that allowed me to finish my degree.

DEDICATION

I would like to thank my loving wife, Giselle (Jaz). You have been my constant companion on this journey. I want to fall more in love with you every day. I also want to thank my little girl, Athena. You help make life worth living and some days were my only reason to continue. I also want to thank my parents, Timothy and Jacqueline. You two taught me the value of hard work and dedication. In addition, I want to thank my sister, Rachel. You may not have enjoyed it, but you were almost always willing to lend me your expertise when needed. Most importantly, I want to thank my lord and savior, Jesus. You are my constant source of strength and ability. I have done my best, and you did the rest.

TABLE OF CONTENTS

AUTHORIZATION TO SUBMIT THESIS	ii
ABSTRACT	iii
ACKNOWLEDGEMENTS.....	iv
DEDICATION.....	v
TABLE OF CONTENTS	vi
LIST OF FIGURES	viii
CHAPTER 1: BACKGROUND.....	1
1.1 INTRODUCTION	1
1.2 WIND POWER: GOOD OR BAD?	1
1.3 WATER: A SUPERIOR PRIME MOVER	9
1.4 THE DOUBLY FED INDUCTION MACHINE.....	11
1.5 SUMMARY	12
1.6 REFERENCES.....	13
CHAPTER 2: THE MECHANICAL SYSTEM.....	15
2.1 INTRODUCTION	15
2.2 MECHANICAL OPTIONS	15
2.3 TURBINE SPECIFICATION.....	18
2.4 SIZING AND OPTIMIZATION	22
2.5 SUMMARY	27
2.6 REFERENCES.....	27
CHAPTER 3: ELECTRIC MACHINE DESIGN.....	29
3.1 INTRODUCTION	29
3.2 WINDING THEORY	29
3.3 EQUIVALENT CIRCUIT PARAMETERS.....	32

	vii
3.4 THE DESIGN PROCESS	39
3.5 THE ACTUAL DESIGN	41
3.6 SUMMARY	42
3.7 REFERENCES.....	43
CHAPTER 4: SIMULATION AND CONTROL.....	44
4.1 INTRODUCTION	44
4.2 ELECTRICAL SYSTEM MODELS	44
4.3 MECHANICAL SYSTEM MODELS.....	48
4.4 CONTROLS.....	49
4.5 SIMULATION RESULTS	54
4.6 SUMMARY	57
4.7 REFERENCES.....	57
CHAPTER 5: CONCLUSIONS	58
5.1 SUMMARY	58
5.2 FUTURE WORK.....	59
APPENDIX A: MATHCAD DFIM DESIGN SHEET	62

LIST OF FIGURES

Figure 1-1. Distribution of Renewable Generation Capacity	2
Figure 1-2. Distribution of Renewable Generation Capacity Excluding Hydropower	2
Figure 1-3. Schematic of Fluid Flow Through a Disk-Shaped Actuator.....	3
Figure 1-4. Plot of Wind Generation vs. Load for an Average Day (2013)	5
Figure 1-5. Plot of Daily Averages of Wind Generation vs. Load (2013)	6
Figure 1-6. Wind Turbine Obstruction of the Columbia Gorge Skyline.....	7
Figure 1-7. UEK Low Impact Hydrokinetic Turbine	10
Figure 1-8. Lunar Tidal Turbine by Lunar Energy	10
Figure 1-9. DFIM Based Wind Turbine Topology.....	11
Figure 2-1. Horizontal Axis Turbine Mooring Options.....	17
Figure 2-2. Horizontal Axis Turbine Duct Shape Options	17
Figure 2-3. Side Profile of Hydrokinetic Turbine by Radkey	19
Figure 2-4. Configuration of Baseline Ducted Turbine.....	20
Figure 2-5. Plot of Power Coefficient vs. Tip Speed Ratio for Selected Turbine	21
Figure 2-6. Plot of Approximate Power Coefficient vs. Tip Speed Ratio Curve	21
Figure 2-7. Discharge vs. Velocity and Height Correlation for USGS 12391950	23
Figure 2-8. Photo of USGS 12391950.....	25
Figure 2-9. Velocity Duration Curve for USGS 12391950.....	25
Figure 2-10. Power Duration Curves for USGS 12391950.....	26
Figure 2-11. Daily Average Power Distribution USGS 12391950	26
Figure 3-1. DFIM Steady State Equivalent Circuit	32
Figure 3-2. Generic Slot Geometry with Double Layer Winding	36
Figure 3-3. DFIM Geometry within Duct Ring.....	39
Figure 3-4. Power vs. Speed Curve for Designed DFIM with Shorted Rotor.....	42
Figure 4-1. Simulation Block Diagram of DFIM Dynamic Model	46
Figure 4-2. Topology for Ideal Switching Model of Two Level VSC	47
Figure 4-3. Simulink [®] Model of Rotational Speed Controller	51
Figure 4-4. Simulink [®] Model of Current Reference Calculator	52
Figure 4-5. Simulink [®] Model for the Current Control Loop.....	53

Figure 4-6. Mechanical Rotational Speed Comparison Plot	55
Figure 4-7. DFIM Stator and Rotor A Phase Current Plots.....	55
Figure 4-8. DFIM Real and Reactive Power Plots	56

CHAPTER 1: BACKGROUND

1.1 INTRODUCTION

The United States of America is at a crossroads regarding its energy policy. Many Americans are calling for energy independence while, simultaneously, demanding more environmentally friendly electric generation. How can this country fulfill these demands? Many states have taken it upon themselves to pass legislation or regulations to try to force utilities to meet at least the second demand of new environmentally friendly generation. From a quick Wikipedia search, it can be seen that almost three quarters of the states have established some sort of Renewable Portfolio Standards (RPS) program [1]. An extreme example of these programs comes from the State of New York where, in early 2010, the Public Service Commission established a new RPS standard requiring that 30% of the state's energy generation come from renewable sources by the year 2015 [2]. These new standards are not localized to states controlled by a single political party. In Texas, a conservative stronghold, the Public Utility Commission has set forth rules requiring 5,880 MW of installed generating capacity from renewable energy sources by January 1, 2015, with the additional goal of having the means available to reach 10,000 MW by the year 2025 [3]. In light of these new regulations, renewable energy sources are in high demand, but which ones should be used? One rapidly growing choice is wind generation, but is this the best option?

1.2 WIND POWER: GOOD OR BAD?

No one can deny the rapid growth of wind power generation in the United States. From 1999 to 2013, installed wind generation capacity has increased from 2,472 MW to 61,108 MW, an increase of 2,372% [4]. There are two types of wind power generation, onshore and offshore. Onshore wind is the primary wind generation in the U.S. and is the second largest renewable resource behind conventional hydropower, which many people choose not to include. As of 2011, onshore wind made up over 32% of the renewable generation capacity when including hydropower and almost 72% when it is excluded [5]. The full renewable generation capacity distributions can be found in Figure 1-1 and Figure 1-2 which were created using 2011 net summer capacity data from all users gathered from the U.S. Energy Information Administration [5].

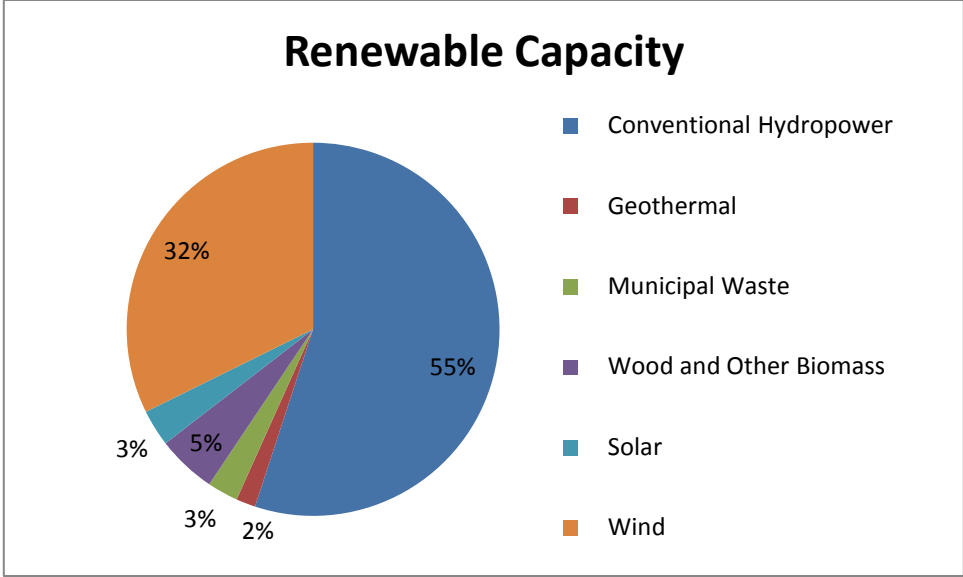


Figure 1-1. Distribution of Renewable Generation Capacity

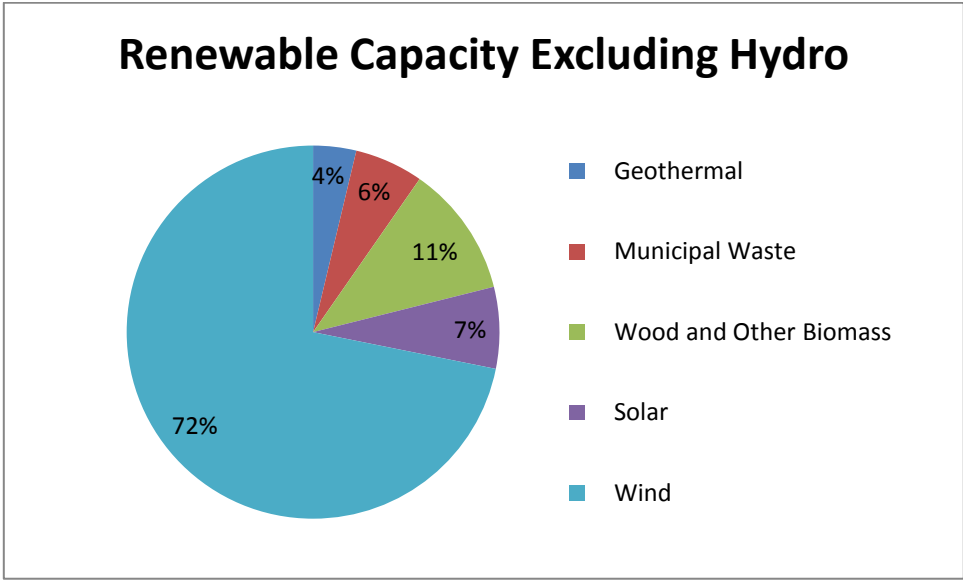


Figure 1-2. Distribution of Renewable Generation Capacity Excluding Hydropower

Many policymakers and private citizens, including the current President, have become champions for onshore wind power generation in the United States, but there are several drawbacks to this technology and its application that they fail to understand and/or consider. A few of these issues will be discussed in some detail in the following paragraphs, including failures and inadequacies in standard design practices, variability and reliability in actual generation, as well as issues regarding placement and natural resource usage. Offshore wind

generation, is not plagued by as many issues as onshore generation, but has not become popular in the United States [5].

Many engineers, especially electrical engineers, use a theory sometimes referred to the actuator disk theory to examine the potential energy available in the wind as well as its extraction. This is the primary theory presented in two prominent electrical engineering texts on technologies to assist in wind power generation and can be reviewed in references [6] and [7]. This theory explains the extraction of kinetic energy from a moving fluid using conservation of energy, the theory of momentum, and the application of Bernoulli's Equation. Reference [6] explains that "The rotor wind capturing energy is viewed as a porous disk, which causes a decrease in momentum of the airflow, resulting in a pressure jump in the faces of the disk and a deflection of downstream flows". This concept is illustrated in Figure 1-3 which was taken from the same reference.

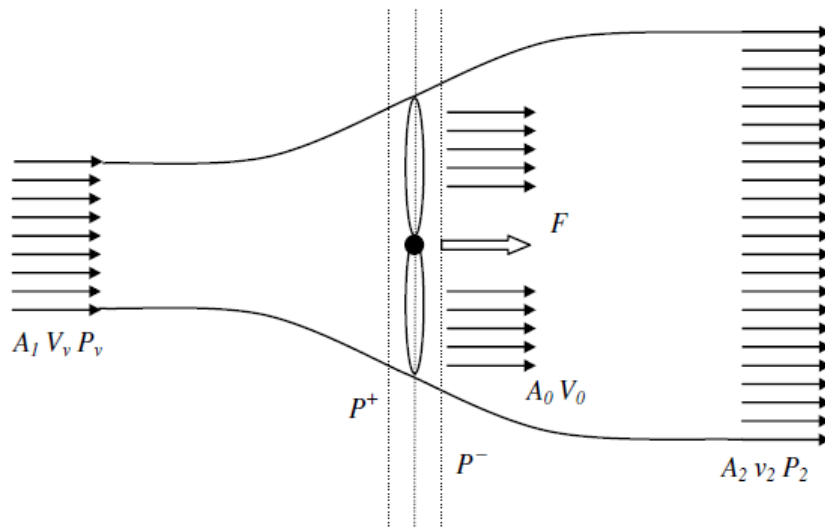


Figure 1-3. Schematic of Fluid Flow Through a Disk-Shaped Actuator [6]

This theory can be summed up in two equations. Equation (1.1) is the total power, P_v , from the kinetic energy crossing through an area A_1 , where ρ is the density and V_v is the speed of the airflow.

$$P_v = \frac{1}{2} \cdot \rho \cdot A_1 \cdot V_v^3 \quad (1.1)$$

The actual power that the wind turbine can extract, P_t , is described by (1.2).

$$P_t = \frac{1}{2} \cdot \rho \cdot A_0 \cdot V_v^3 \cdot C_p \quad (1.2)$$

Where A_0 is the area swept by the turbine blades and C_p is a dimensionless parameter known as the power coefficient. This coefficient is dependent on the geometry of the turbine and is a function of the rotational speed of the turbine, wind speed, and the pitch of the blades. The theoretical max percentage of the total available kinetic energy that can be harnessed is related to the Betz limit which is 59.3% for this given geometry [6].

In order to use the actuator disk theory, there are several assumptions that must be made, none of which are actually valid. The most invalid of these assumptions is that air is an incompressible substance [6]. A truly incompressible fluid is one where density is constant regardless of temperature and pressure. In contrast, air can often be modeled as a ideal gas. Equation (1.3) is one form of the ideal gas equation of state.

$$p \cdot V = mR \cdot T \quad (1.3)$$

In this formula, p is pressure, V is volume, m is mass, R is a gas constant defined as the universal gas coefficient divided by the molecular weight of the substance, and T is the temperature in Kelvin [8]. Since mass is equal to density times volume, the ideal gas law can be rewritten as (1.4) where ρ is density.

$$\rho = \frac{p}{R \cdot T} \quad (1.4)$$

If pressure is assumed to be a function of elevation and therefore constant at a single location, it can be seen that density varies inversely with temperature. R for dry air is 0.2870 kJ/(kg*K) [8]. Assuming 1 atm of atmospheric pressure, it can be seen that the density of air increases over 20% from 100 °F to 0°F. These values are based on an assumption that air is made up of a specific mixture of gases, but this mixture can vary by specific location. In addition, the density of air will greatly vary depending on the percent humidity. In light of this, a method that assumes air to be incompressible will not be very accurate. For a better model it might be beneficial to use computational fluid dynamics (CFD).

In conventional power generation, such as a coal fired plant, the ability exists to produce almost any value of power output at any time, up to the nameplate value, although, this is not always how control is done. This means that that most generation is deterministic which allows utilities to generate the exact power necessary to supply the variable loads on their

system. An issue with many renewable energy sources is that they are more stochastic and behave more like the variable load. This is because their generation capacity is subject to the availability of their source whether it be wind, sunlight, or something else. This variability can be problematic to the utilities' systems, both in operation and planning. These problems only grow if this variability cannot be predicted for short and/or long term operation.

Power generated from the wind is very erratic in nature. It has the ability to dramatically change value over the course of a single day and from day to day. In addition, wind generation tends not to line up with system load both daily and seasonally. To demonstrate these issues, data was obtained from Paul Ortmann, a senior electrical engineer in the Power Quality Department at Idaho Power. This data includes values for total wind power generation and system load on Idaho Power's entire system in ten minute intervals for more than a year. Two figures were generated using this data to highlight problems with wind generation. Figure 1.4 shows an average day created by averaging each individual time period over the course of a single year, 2013 [9].

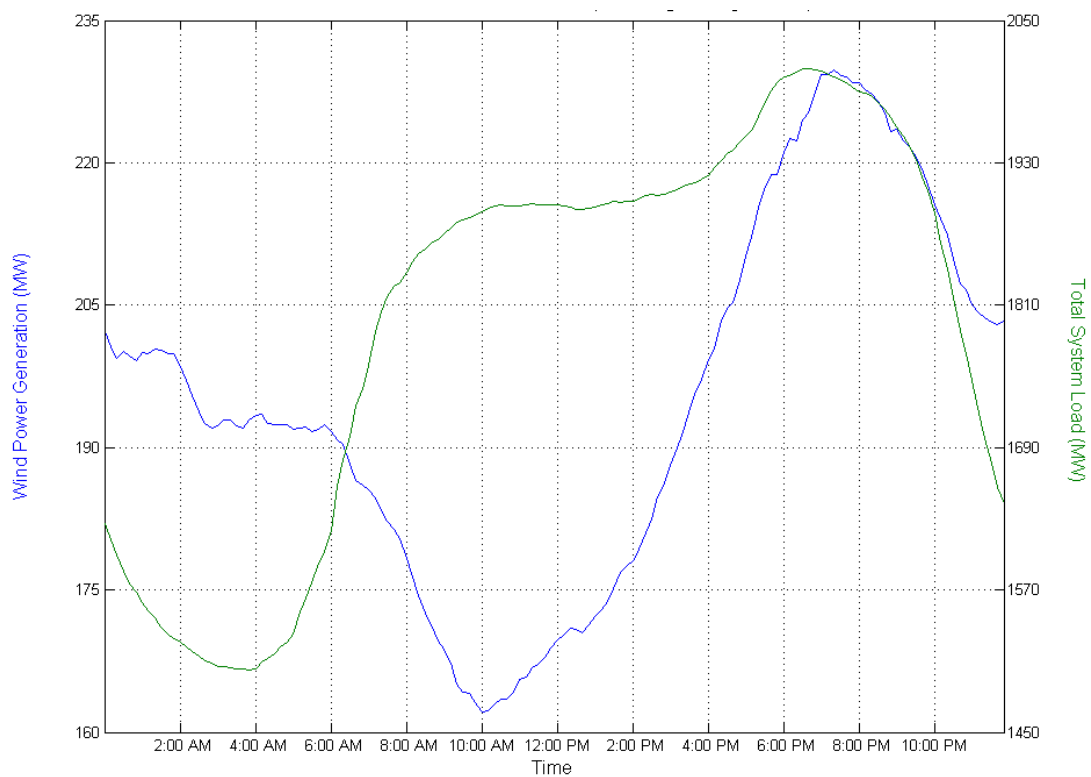


Figure 1-4. Plot of Wind Generation vs. Load for an Average Day (2013)

The shapes of these two curves do not match. The two peaks differ by almost an hour, and that is not the biggest problem. At least in Idaho's System, a large part of the energy generated from wind is produced during the night when load experiences its daily low. Likewise, wind power generation experiences its daily minimum during the middle of the day while load is high. Figure 1-5 displays daily averages over the course of a year [9].

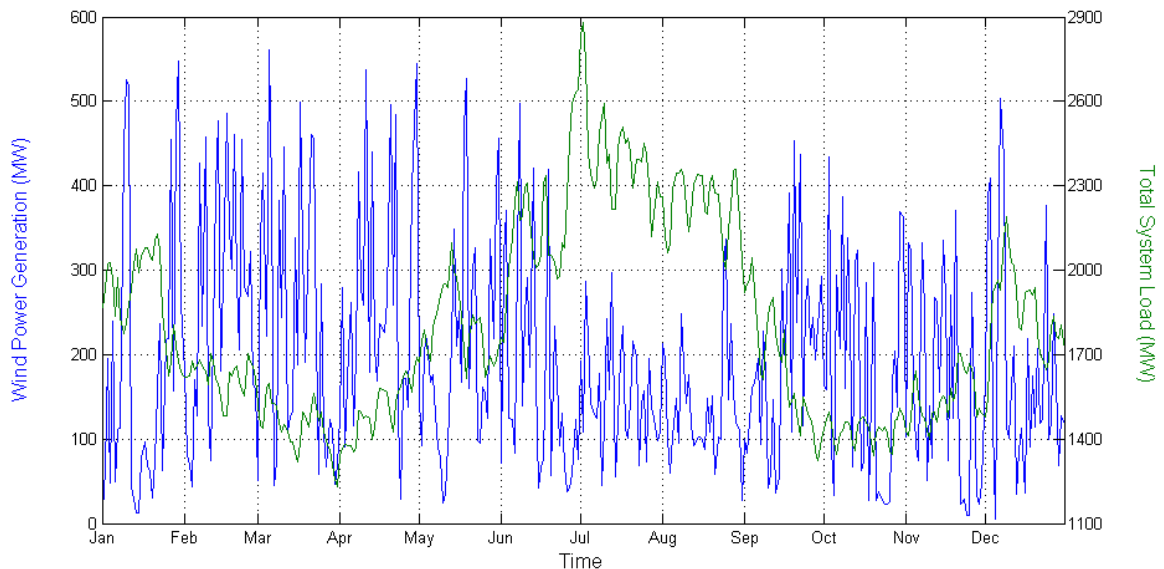


Figure 1-5. Plot of Daily Averages of Wind Generation vs. Load (2013)

Figure 1-5 highlights two problems. The first is the same mismatch seen on the daily plot, only here it becomes apparent that wind generation is minimal during the summer months where load peaks for the year, in part due to air conditioners used to cope with the Idaho heat, as well as, according to Dr. Brian K. Johnson, irrigation load which begins shutting down in July and August. More importantly, this plot highlights how variable wind can be. Wind generation oscillates wildly from one day to the next with minimum and maximum generation for the year within days of each other. This becomes worse when the lack of exact predictability is taken into account. Wind generation highly depends on the weather which is difficult to accurately predict. If reserve generation sources are available, they can compensate for wind's variability, but these may have increased cost or pollution.

Another growing concern about wind turbines is their placement. The ideal location for new wind farms would be in open, undeveloped, locations with above average wind speed, but with the ability for grid connection. This is leading wind farm developers to construct farms

in areas closer and closer to federally protected lands. For example, consider the Columbia River Gorge National Scenic Area established in 1986 along the Columbia River including portions of both Oregon and Washington. As of yet, it does not appear that any wind farm projects have been approved within the scenic area, which makes sense considering many would see it as a violation to the Columbia River Gorge Commission's mission "To protect and enhance the scenic, natural, cultural and recreational resources of the Columbia River Gorge; and to protect and support the economy of the area by encouraging growth to occur in urban areas and allowing future economic development consistent with resource protection" [10]. Unfortunately, new wind farms have been and are being constructed in close proximity which, although not in the defined area, are having affects on the scenic, natural, cultural, and recreational resources. Wind farms are visual pollution that is disrupting protected scenic vistas, many of which have been nearly unchanged in over a century. If proof is desired, simply drive along one of the major roads that passes through this protected scenic area. Figure 1-6 is a photo taken in March of 2014 while driving through the Gorge along Washington State Route 14 .



Figure 1-6. Wind Turbine Obstruction of the Columbia Gorge Skyline

Some individuals may be less upset about this disruption than others. Some may even find these shiny white feats of engineering as beautiful gems on the hillside, but that is today. What will these turbines look like in twenty or so years when they reach the end of their useful lives? Will the companies that installed them have the funds to take them down, will they even still exist?

In addition to the visual issues, several environmentalist groups and individual citizens are becoming concerned with the impact the construction and operation of wind farms are having on the habitats of indigenous species. The Whistling Ridge Energy Project is one example where wind farm developers have encountered extreme resistance to their project. This development has been challenged by multiple organizations including the Friends of the Columbia Gorge and Save Our Scenic Area. These groups went so far as to challenge gubernatorial approval in the Washington State Supreme Court; their main arguments revolving around their belief that the project would "mar world-class scenery and harm endangered species habitat" [11]. In addition to their concerns about how the placement of 50, 426 ft tall, wind turbines on prominent ridgelines might affect tourism, this project will require the destruction of hundreds of acres of forest within a specifically designated Northern Spotted Owl Special Emphasis Area. The Northern Spotted Owl is currently considered an endangered species [11].

With these growing controversies and the initial desire for easy and cheap grid connectivity, it might seem in the best interest of wind developers to move their farms closer to more populated areas, but that is not free of issues. There are growing indications that the noise created by wind farms may actually have ill effects on the health of individuals living nearby. Some commonly reported symptoms believed to be associated with these noise emissions include "altered quality of life, sleep disturbance, excessive tiredness, headache, stress, and distress", and other reports included "migraines, hearing problems, tinnitus, heart palpitations, anxiety, and depression" [12]. Several organizations are beginning to acknowledge these connections. In 2011, the Ontario Environmental Review Tribunal made the decision to accept this connection, but left extent of impact up for debate [12].

With all of these problems, issues, and controversies, it should be apparent that onshore wind is certainly not the best solution for fulfilling, growing environmentally friendly, energy demands. What would be a better solution, and what should be done with all of the technology developed to improve wind generation? Should it be abandoned, or is there a better application?

1.3 WATER: A SUPERIOR PRIME MOVER

Seeing that wind is not a viable option, it is time to reevaluate a more consistent and historically trusted prime mover. Water is a source of work and energy that has been used for more than a millennium. The first actual hydroelectric power plant was established in the United States over 130 years ago in Appleton, Wisconsin [13]. Conventional hydroelectric generation makes up about 55% of renewable energy generation and approximately 10% of all generation in the U.S. [5] [13]. Why not take the advancements made for the wind energy sector and apply them to new in-stream hydroelectric generation applications?

Unlike air, in nature, water is practically an incompressible fluid. Most liquids exhibit low compressibility, but water exceeds almost all of them. Even in the ocean at a depth where the pressure is 150 times atmospheric, water compression is less than one percent [14]. This means that water flow will fit into the standard actuator disk theory much better than air, although a CFD analysis may still offer additional improvement.

In addition, water is significantly denser than air. Using (1.4) and the value of R from Reference [8] it can be seen that the density of air at 50°F is approximately 1.25 kg/m^3 . Knowing that water at the same temperature is about 1000 kg/m^3 , the density of water is around 800 times that of air. This means that a water turbine could produce the same power as a wind turbine with a swept area $1/800$ times the size given the same velocity, or approximately a tenth the velocity for the same area. The increased density of water can also help to avoid rapid changes in speed as seen with wind flows. A larger density results in a larger inertia which helps to mitigate large, rapid, changes in stream velocity much like how an inductor mitigates large, rapid, changes in current flow within a circuit.

Water flows, like those in rivers, are far more predictable than air flow, in part, because they vary more seasonally than day to day. For example, most rivers in the U.S. have an increased discharge in late spring and early summer during runoff season from the mountains. The flow of water is much more likely to follow historical trends. In addition, if in-stream generators are placed downstream of existing dams, the exact discharge will be known as it is controlled by them.

In-stream hydroelectric generation, or hydrokinetic generation as it is sometimes referred, is by no means a new technology. There has been commercial and government research in this area for more than 30 years. This has resulted in several commercial models from multiple companies. One example would be the UEK, Underwater Electric Kite, low impact hydrokinetic turbines as shown in Figure 1-7 [15].

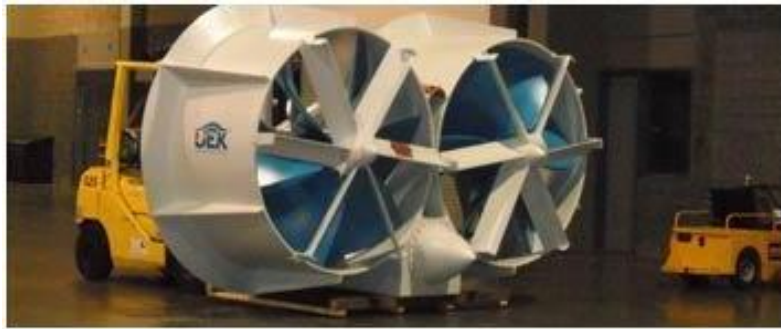


Figure 1-7. UEK Low Impact Hydrokinetic Turbine [15]

Another example would be the LTT, Lunar Tidal Turbine, sold by a company called Lunar Energy out of the United Kingdom. This turbine is a bidirectional turbine that is housed in a symmetrical venturi duct and was designed, as the name suggests, for harnessing energy from the tides. An illustration of the LTT can be found in Figure 1-8 [16].



Figure 1-8. Lunar Tidal Turbine by Lunar Energy [16]

1.4 THE DOUBLY FED INDUCTION MACHINE

A literature review shows that the main focus of research regarding in-stream hydroelectric generation is focused on improving the actual mechanical system. Wind generation research has put a much larger focus on the design of different and more efficient electrical systems in addition to mechanical improvements. Some of these electrical systems can be applied in order to improve hydrokinetic generation.

Prior to the mid-1990s, most wind turbines made use of the squirrel cage induction machine directly connected to the power grid and therefore were fixed speed turbines. As the wind industry began to grow, focus shifted towards designing variable speed wind turbines. Today, most of these variable speed turbines are based on the doubly fed induction machine (DFIM), although it shares the market with wound rotor synchronous generators and permanent magnet synchronous generators [6]. The DFIM "is essentially a wound rotor induction generator in which the rotor circuit can be controlled by external devices to achieve variable speed operation" [7]. This machine is controlled by applying variable magnitude voltage and frequency to the rotor circuit through a bidirectional power electronic converter. Figure 1-9 shows the topology of traditional DFIM connections.

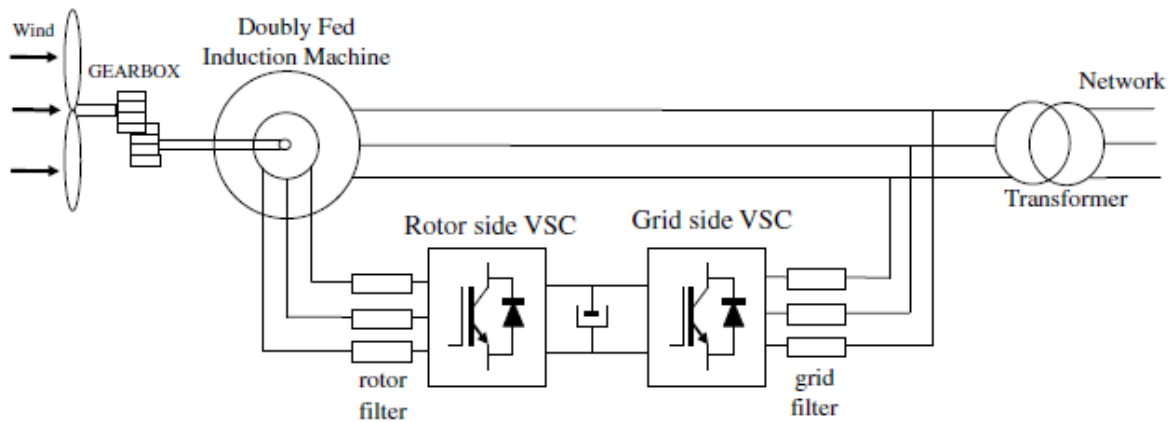


Figure 1-9. DFIM Based Wind Turbine Topology [6]

There are several features of the DFIM that could help improve the performance of the overall water turbine. One such feature is a speed range of -30% to +20% synchronous speed[6]. This allows for higher efficiency to be maintained over a larger water speed range. The rotor is usually designed for a power of approximately 30% of the stator rated power,

effectively allowing the machine to generate 130% rated power for higher speeds. This reduced sized converter is cheaper and has lower losses, and therefore better efficiency, than the full converter required when using either of the synchronous machine options for variable speed operation. This machine offers complete control of both real and reactive power. It allows for the production or absorption of reactive power through both the stator and grid side converter [7].

As shown in the figure above, most DFIM topologies make use of a gearbox to reconcile the low speed of the rotor blades to the higher speed of the generator. These gearboxes pose a liability to the overall system. The gearbox is one of the most expensive parts of the turbine assembly both in initial investment and long term maintenance. These gearboxes are also noisy; the meshing of individual teeth lead to substantial audible noise. Standard efficiencies for gearboxes used in wind applications range from 95% to 98% [7]. That does not seem bad, but if a machine with an efficiency of 98% and gearbox with the same is assumed, the overall efficiency is approximately 96%, doubling overall losses of using the machine alone. It is apparent that eliminating the gearbox would be highly beneficial. This can be achieved by increasing the number of pole pairs to fit (1.5).

$$P = \frac{f_s}{f_m} \quad (1.5)$$

Where P is the number of pole pairs, f_s is the grid frequency in Hz, and f_m is the desired mechanical rotational frequency in Hz. The one drawback to this is that the machine must be large enough in diameter to accommodate the large number of poles. This will be addressed in the design process in Chapter 3.

1.5 SUMMARY

The United States is actively moving to create more environmentally friendly electric power generation. Unfortunately, investors and developers are spending most of their time and money on a technology that is flawed in its very nature. The time and resources that are being invested in wind would be much better spent if used to create new in-stream hydroelectric generation. Although hydrokinetic generation is not a new concept, it can be greatly improved by incorporating advances made for wind generation. One of the greatest improvements that can be made is the use of a gearless doubly fed induction machine. This

will allow for less noise, lower cost, and more overall efficiency. The rest of this thesis highlights this unique application of the DFIM to in-stream hydroelectric generation starting with a more in depth analysis of the mechanical system in the next chapter.

1.6 REFERENCES

- [1] Wikipedia contributors, "Renewable portfolio standard," in *Wikipedia, The Free Encyclopedia*. Wikipedia, The Free Encyclopedia, [online document], 2014. Available: http://en.wikipedia.org/w/index.php?title=Renewable_portfolio_standard&oldid=607098287 [Accessed: June 11, 2014].
- [2] New York State Public Service Commission, "03-E-0188: Renewable Portfolio Standard - Home Page," *New York State Public Service Commission*, 2014. [Online]. Available: <http://www3.dps.ny.gov/W/PSCWeb.nsf/All/1008ED2F934294AE85257687006F38BD>. [Accessed: June 11, 2014].
- [3] Public Utility Commission of Texas, "§25.173. Goal for Renewable Energy," *Public Utility Commission of Texas*, 2009. [Online]. Available: <http://www.puc.texas.gov/agency/ruleslaws/subrules/electric/25.173/25.173.pdf>. [Accessed: June 11, 2014].
- [4] U.S. Department of Energy, "Installed Wind Capacity," *U.S. Department of Energy*, 2014. [Online]. Available: http://apps2.eere.energy.gov/wind/windexchange/wind_installed_capacity.asp. [Accessed: June 11, 2014].
- [5] U.S. Energy Information Administration, "Annual Energy Outlook 2013," *U.S. Energy Information Administration*, 2013. [Online]. Available: <http://www.eia.gov/oiaf/aeo/tablebrowser/#release=AEO2013&subject=10-AEO2013&table=16-AEO2013®ion=0-0&cases=ref2013-d102312a>. [Accessed: June 11, 2014].
- [6] G. Abad et al., *Doubly Fed Induction Machine: Modeling and Control for Wind Energy Generation Applications*. Hoboken, NJ: Wiley-IEEE Press, 2011.
- [7] B. Wu et al., *Power Conversion and Control of Wind Energy Systems*. Hoboken, NJ: Wiley-IEEE Press, 2011.

- [8] M. Moran et al., *Fundamentals of Engineering Thermodynamics*, 7th ed. Hoboken, NJ: John Wiley & Sons, Inc., 2011.
- [9] P. Ortmann, "Requested data," Personal email (June 13, 2014).
- [10] Columbia River Gorge Commission, *Columbia River Gorge Commission*, 2014. [Online]. Available: <http://www.gorgecommission.org/>. [Accessed: June 12, 2014].
- [11] Friends of the Columbia Gorge, "Stop the Whistling Ridge Energy Project", *Friends of the Columbia Gorge*, 2013. [Online]. Available: <http://www.gorgefriends.org/article.php?list=type&type=56>. [Accessed: June 12, 2014].
- [12] R. Jeffery et al., "Adverse health effects of industrial wind turbines," *Canadian Family Physician*, vol. 59, no. 5, May, 2013. [Online Serial] Available: <http://www.cfp.ca/content/59/5/473.full>. [Accessed: June 12, 2014].
- [13] Office of Energy Efficiency & Renewable Energy, "History of Hydropower," *U.S. Department of Energy*, 2014. [Online]. Available: <http://energy.gov/eere/water/history-hydropower>. [Accessed: June 13, 2014].
- [14] United States Geological Survey, "Water Compressibility," *USGS: Science for a Changing World*, 2014. [Online]. Available: <http://water.usgs.gov/edu/compressibility.html>. [Accessed: June 13, 2014].
- [15] UEK Systems, *UEK Underwater Electric Kite*, 2010. [Online]. Available: <http://uekus.com/>. [Accessed: June 13, 2014].
- [16] Lunar Energy Power Limited, "Product Overview," *Lunar Energy*, 2010. [Online]. Available: <http://www.lunarenergy.co.uk/productOverview.htm>. [Accessed: June 13, 2014].

CHAPTER 2: THE MECHANICAL SYSTEM

2.1 INTRODUCTION

The biggest problem with electrical designs today is that the engineers involved do not have a sufficient understanding of the mechanical system with which their electrical system will be coupled. In order to help the reader have sufficient knowledge of the overall system, this chapter is presented to inform them on the mechanical aspects related to in-stream hydroelectric turbines. This chapter is broken up into three main sections. The first section presents several options available to someone looking to design a hydrokinetic turbine. The second section provides details relating to the actual turbine chosen for this specific application. Finally, the last section focuses on refining the mechanical design to optimize stream usage as well as choose the best location.

2.2 MECHANICAL OPTIONS

The design of the mechanical portion of a hydrokinetic turbine is more complex than most electrical engineers would imagine as there are many options that affect the construction, performance, and overall efficiency of the turbine. Some of these options involve the rotor configuration, mooring options, and channel augmentation.

The rotor configuration is the most important of the mechanical options, as it is the rotor blades that are responsible for taking the kinetic energy from the velocity of the stream and converting it into rotational mechanical energy that can be used by the electric machine to produce electricity [1]. The rotor configuration can be broken down into two main parts: the first being the turbine or blade orientation and the second part being the exact number of blades.

In terms of orientation, there are three main types of in-stream hydroelectric turbines. These include the horizontal axis, vertical axis, and cross-flow turbines. Turbines typically referred to as horizontal axis turbines are the same configuration used in most onshore wind farms. With these turbines, water flow is perpendicular to the area swept by the blades which means that the water flow is parallel to the axis of rotation. Where a horizontal turbine is defined by its orientation with water flow, a vertical turbine is better defined by its

orientation to the surface of the water. A vertical axis turbine is one in which the area swept by its blades is parallel the water's surface, the axis of rotation is perpendicular. A cross-flow turbine is more closely related to the horizontal than vertical axis turbines. The main difference between the two is that the water flow is perpendicular to the turbine's axis of rotation. These turbines are similar in design to old water wheels [2]. In the rest of this thesis, the horizontal axis turbine will be the main focus as 43% of all current hydrokinetic turbines are of this type and vertical axis turbines, which make up 33%, have been effectively discarded by the greater wind energy industry [3]. There is some focus in this thesis on methods used for wind, as they have made many technological advances that may be useful of in-stream hydroelectric generation.

Equally important to the orientation is the decision of how many blades to actually use. For in-stream turbines two and three blades are the most common although some have even more [2]. Single blade turbines are a bad idea as they will "have an asymmetrical mechanical load distribution" and aerodynamic imbalance which can produce mechanical vibrations that may damage or fatigue other components in the turbine system and reduce its overall lifespan [1]. The use of two blades may have popularity because the fewer blades used means a higher rotational frequency which, in turn, means that a lower gear ratio may be used. A lower gear ratio means less cost. The three blade design is by far the most popular in the wind industry. Fewer blades may reduce cost, both for the blades themselves and the gearbox, but the higher speeds that come as a result produce more acoustic noise which can be harmful. Turbines with more than three blades are not common, in part, because the increased cost, but also because, with more blades, each blade must be closer to its neighbors. Each blade produces a lagging turbulence. When the blades are closer this turbulence can have damaging effects on the other blades [1].

Another option to consider is the mooring of the turbine, or how it is held in place. There are four main types of mooring used with hydrokinetic turbines. These main types can be seen in Figure 2-1: a) inclined axis, b) rigid mooring, c) floating with a non-submerged generator, and d) floating with a submerged generator.

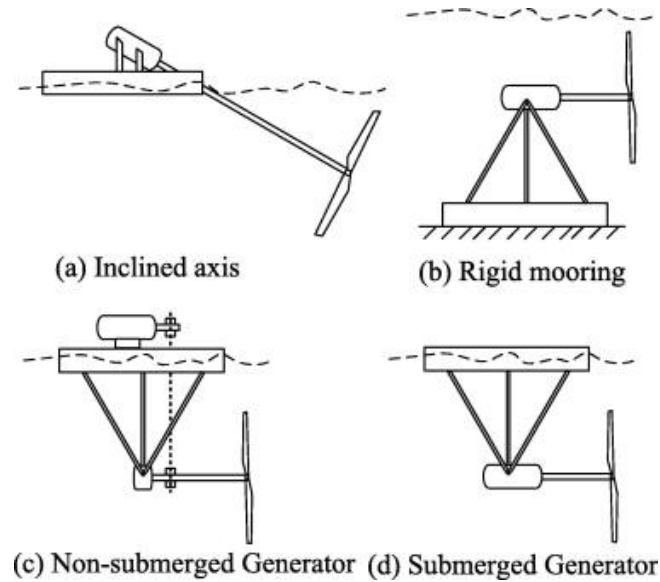


Figure 2-1. Horizontal Axis Turbine Mooring Options [3]

When picking a mooring option there are various tradeoffs relating to simplicity and ease of construction of the mounting structure, water proofing of the turbine, and dealing with competing users such as boats [3].

Another important option to consider in hydrokinetic turbine design is whether to perform channel augmentation. Adding a duct to the turbine is the most common way of implementing augmentation. There are several options for adding a duct to a horizontal axis turbine, three of which can be seen in Figure 2-2 taken from [3] with minor modifications.

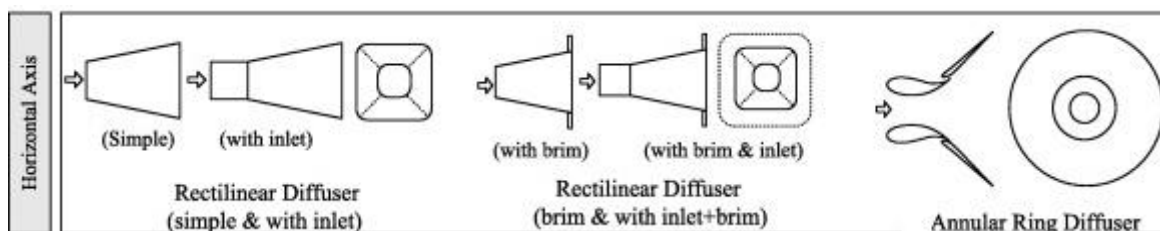


Figure 2-2. Horizontal Axis Turbine Duct Shape Options [3]

Evidence shows that the addition of these ducts increases the total amount of power that can be captured by the turbine [3]. There are several explanations for why adding this duct causes improvements. Reference [3] claims that the "augmentation channels induce a sub-atmospheric pressure within a constrained area and thereby increase the velocity". From a discussion with a fellow graduate student with an undergraduate degree in mechanical

engineering, a possibly better answer was attained. Turbines, by nature, reduce the pressure on the back of the blades in comparison to the front. Since without a duct, the turbine is open to the flow, the pressure a short distance behind the turbine will be equal to that in front, therefore there is a large pressure difference over a small distance that will cause separation, which is a source of loss in efficiency. A duct is essentially a diffuser. A diffuser acts to decrease velocity and increase pressure. This allows pressure to gradually increase from the backside of the turbine blades to the outlet of the diffuser. If designed correctly, this diffuser will allow for a lower pressure on the backside of the blades while preventing separation, effectively increasing the energy harnessed by the turbine while decreasing losses. A report prepared for the U.S. Department of Energy in 1981 by Aerovironment, Inc. seems to support this claim. When designing a ducted option, their optimum design point was contingent on preventing separation [4]. According to [3], the addition of a diffuser can cause the power coefficient to grow as high as 1.69.

Many engineers would immediately disregard these large power coefficients as they are above 0.593, the Betz limit. The Betz limit is dependent on geometry; this specific value is that for a free flow turbine as modeled with the actuator disk theory [2] [4]. Different types of ducted turbines can have higher values for their Betz limits because of their geometry. A casual observer still needs to be careful to avoid being deceived. There are two different power coefficients when discussing ducted turbines, C_{pa} and C_{pe} . C_{pa} is calculated using only the area swept by the turbine blades and neglects the duct, where C_{pe} is calculated using the entire area taken by the turbine, both aperture and duct [4]. Reference [3] does not state whether 1.69 is a C_{pa} or a C_{pe} , but C_{pa} would be a good assumption as the coefficient is greater than one.

2.3 TURBINE SPECIFICATION

For this application it is important to specify an actual turbine to be coupled to the doubly fed induction machine. Originally, one of the goals of this thesis was to design a mechanical system optimized to work with the DFIM, but after a literature review, a basic fluids course, and a course in computational fluid dynamics, it became apparent that this design would be beyond the scope of an electrical engineering thesis and would be better covered in a mechanical engineering thesis or dissertation.

Without the ability to create a completely new design, it became necessary to find a preexisting turbine design to use in this application. Most literature from hydrokinetic turbine manufactures fails to provide detailed information on their systems. This is most likely for proprietary reasons. Several companies were contacted via email including UEK and Lunar Energy in hopes that they would be willing to share data on their turbines to help advance the field. No replies were ever received.

Without help from industry, the only option was to fall back on a turbine design proposed in *Definition of cost effective river turbine designs: final report for the period September 30, 1980 - December 31, 1981* written by Robert Radkey and Bart Hibbs, this is [4]. Radkey proposed a two bladed, ducted, turbine with an overall diameter of 10 ft, approximately 3.05 m, including the duct. For simplicity and less overall system cost, his design had no active control of the mechanical system such as blade pitching, but instead relied on progressive blade stall for power limiting. A sliced side view of his overall design can be found in Figure 2-3.

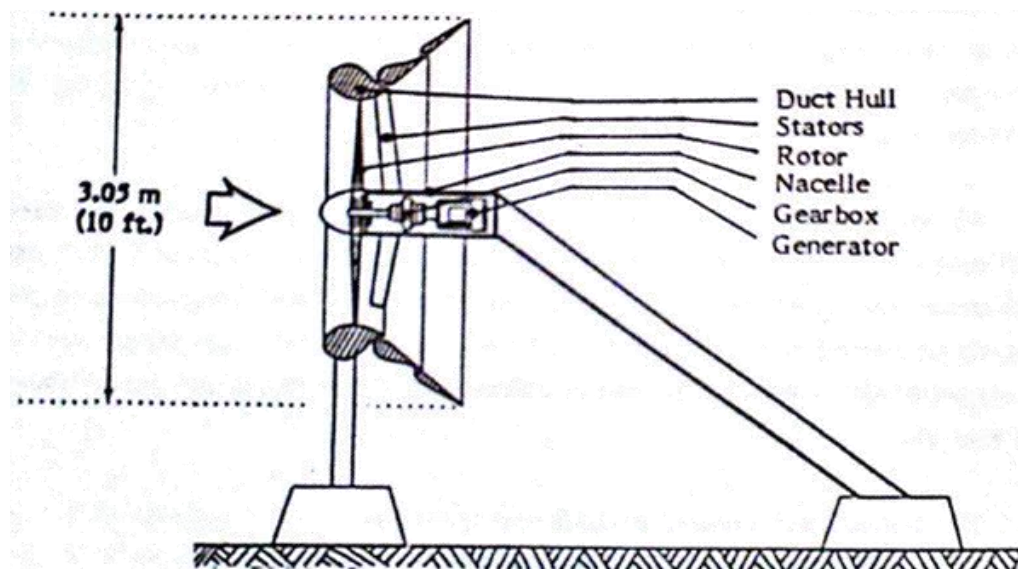


Figure 2-3. Side Profile of Hydrokinetic Turbine by Radkey [4]

Having the rotor within a duct eliminates tip losses. The duct hydrodynamic design was an iterative process performed by computer to find an optimum solution that prevented separation. The proposed design made use of an annular ring diffuser broken into three sections which can be better examined in Figure 2-4.

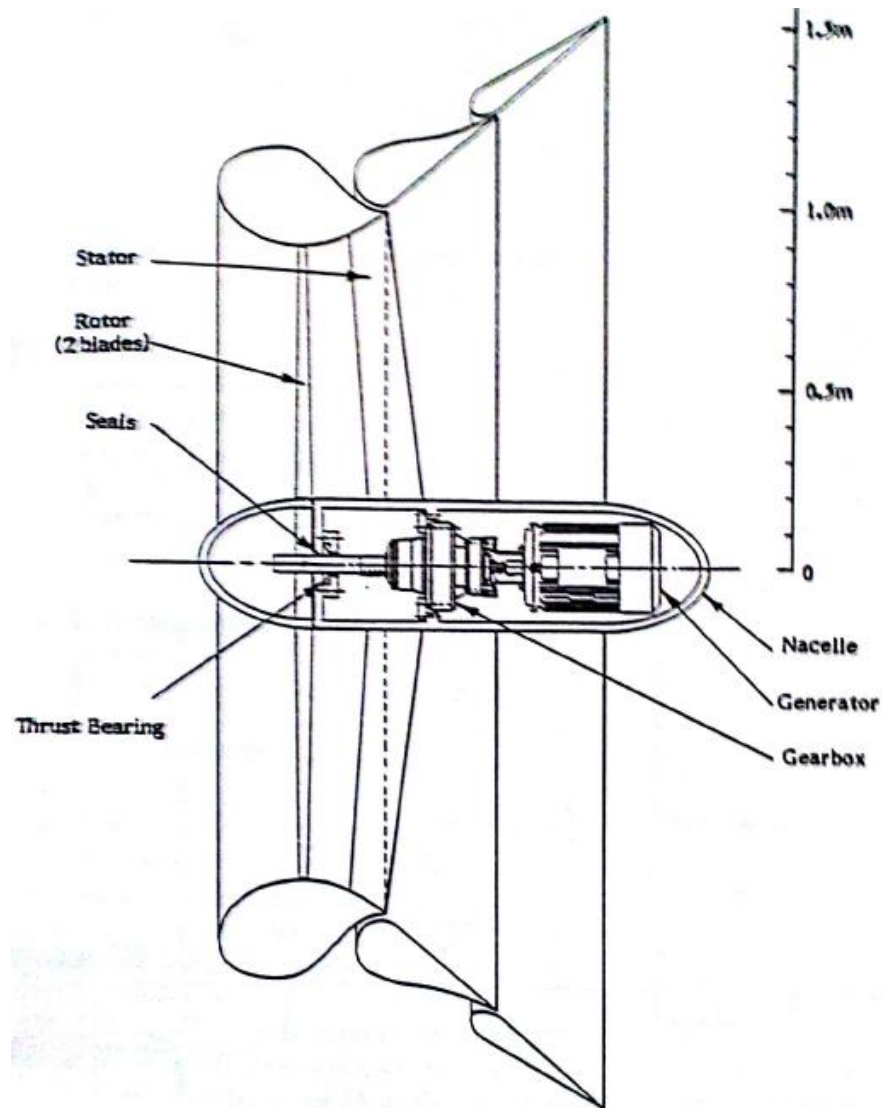


Figure 2-4. Configuration of Baseline Ducted Turbine [4]

Figure 2-4 is to scale and can be used to determine other parameters, such as the blade length from the center of the shaft to the tip which is approximately 0.871 m.

Often turbines are characterized by plots of their tip speed ratio vs. power coefficient. Tip speed ratio, X , is a value relating rotational speed to the speed of fluid flow and is defined in (2.1).

$$X = \frac{\text{Rotational_Speed (Hz)} \cdot \pi \cdot \text{Diameter (m)}}{\text{Fluid_Speed} \left(\frac{\text{m}}{\text{s}} \right)} \quad (2.1)$$

Diameter in (2.1) is that of the cross sectional area swept by the turbine blades, not the outer duct. The plot for Radkey's turbine is presented in Figure 2-5.

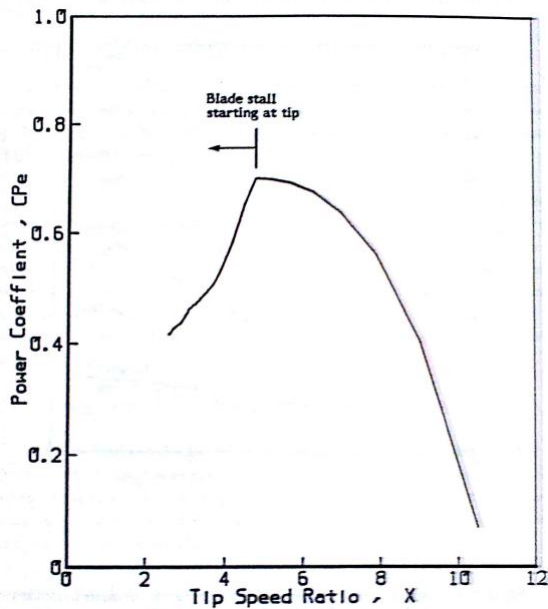


Figure 2-5. Plot of Power Coefficient vs. Tip Speed Ratio for Selected Turbine [4]

The maximum power coefficient for this turbine is 0.7 at a tip speed ratio of approximately 4.75. For simplicity in analysis, data points were taken from Figure 2-5 to create curve fits for the two halves of the plot that could be combined as a complete plot. A plot of this approximate curve can be found in Figure 2-6.

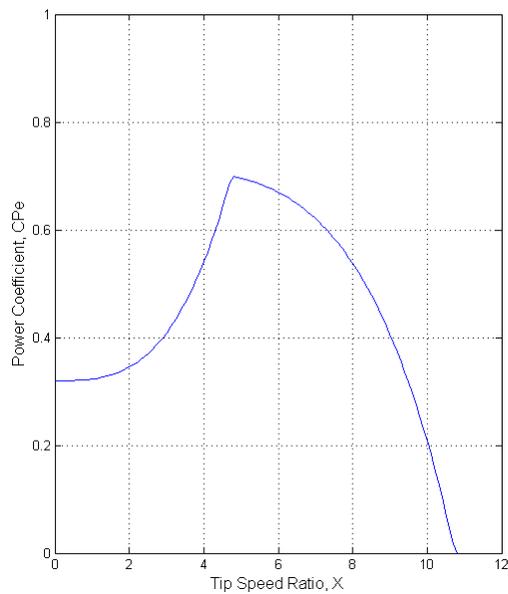


Figure 2-6. Plot of Approximate Power Coefficient vs. Tip Speed Ratio Curve

By scaling this turbine geometrically, based on the overall diameter, it should be possible to scale this turbine and still use this power coefficient vs. tip speed ratio relationship to define its behavior. This is how it was used for analysis in the following section. Some observers may be concerned that the approximate curve includes points below about 2.5 where the actual curve cuts off. This is not a problem with the control algorithm discussed in Chapter 4, the smallest tip speed ratio that will be allowed is approximately 2.9.

2.4 SIZING AND OPTIMIZATION

When implementing an in-stream hydroelectric system, two important parameters to determine are location and machine ratings, both speed and power. There are a couple of ways designers have gone about determining these parameters. Some pick a desired power value and then use location as a variable, looking at locations capable of producing the desired power. Others pick a location and leave the power rating as variable. Still some try to pick both, and then simply check to see if that level of generation is possible. This last method lines up with the method used in [4] more than the other two.

A better solution would be to determine the optimal level of generation for multiple locations, and then pick the location that best fits the desired criteria. That is the approach used in this thesis. Several constraints were set for the design such as a maximum diameter of 3 m, a minimum rated power of 5 kW, a minimum capacity factor of 0.25, and that it must be located in the State of Idaho. The capacity factor is a ratio of actual generation averaged over a period of time, such as a year or multiple years, divided by the nameplate rating of the generator [4]. According to Dr. Brian K. Johnson, 0.25 is about the capacity factor of a good wind turbine.

For this thesis data was acquired from the United States Geological Survey, USGS. This idea to get data from the USGS came from the Radkey report. For that report, the USGS field offices were contacted directly to obtain site data. In the modern era, USGS site data is available on the internet. Reference [5] is a website hosted by the USGS that provides data on all of their river measurement sites including instantaneous stream data taken in 15 minute intervals by automated sensors as well as sporadic manual measurements. At the time the data was taken from this website, most of the sites in Idaho only had instantaneous

discharge data for a time period greater than a year. In order to determine the potential of a site, it is necessary to have data on velocity and height. According to [4], the USGS used Form 9-207 to take measurements multiple times during a year, allowing for the comparison of discharge with velocity and height data. That report used this data to create a function to calculate velocity from discharge. Although that form has been retired, this information is also available on the website. In this thesis, MATLAB[®] was used to find correlations between discharge and both velocity and height values. For most streams both of these parameters appeared to fit a specific type of power plot. Examples of these curves are shown in Figure 2-7.

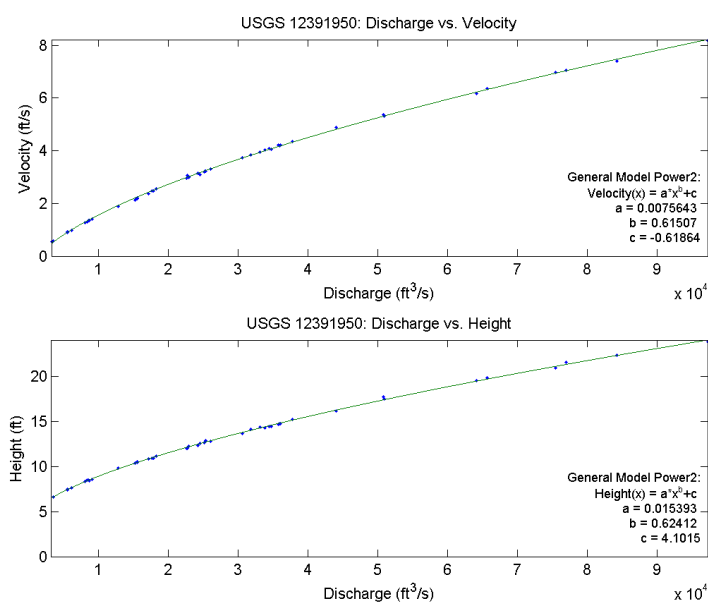


Figure 2-7. Discharge vs. Velocity and Height Correlation for USGS 12391950

With these correlations, it is possible to approximate values for velocity and height using the instantaneous discharge data.

One way [4] looked at examining the potential of a stream was through duration of velocity. The duration of velocity is a way of aligning a specific velocity with the percent of time that the velocity of the stream is equal or greater to it. This concept of duration can be applied to other values such as height and generated power.

To help analyze the individual streams and rivers, a MATLAB[®] program was developed. This program would load the data for a specific site and start by generating the correlations

discussed above. It would then take the instantaneous discharge data and create daily averages over the whole period of continuous data. For example, every data point from every January 1st within the span of data was averaged to create a January 1st value, and likewise for everyday of the year. This was done to save overall processing time. This daily discharge data were then converted to height and velocity data using the correlation. The next step was to generate the duration of velocity and duration of height data. The diameter of the turbine was then fixed at the point where it was equal to the height correlating to a 90% duration. This means that for at least 90% of the year, the turbine will be completely submerged. Next the program began systematically stepping through various duration percentages, setting the rated velocity of the turbine to match the average value of the velocities greater than the correlating stream velocities. The number of pole pairs was then calculated using an amalgamation of (1.5) and (2.1), setting the tip speed ratio, X , to 4.75. Rated power was determined using (1.2) with C_p set to 0.7. Since 0.7 is a C_{pe} , A_0 must be the total area of the turbine including duct. Next, each individual data point was sent through a set of criteria that determines what the mechanical speed should and can be to maximize mechanical power input without exceeding 130% of rated, and setting power to zero when the turbine was not completely submerged or when rotor power exceeded 30% of the total rating. These power data points were then averaged and divided by the rated value to determine the capacity factor. If the capacity factor for this duration percentage was greater or equal to 0.25, an optimization value was calculated using (2.2).

$$\text{Opt} = \left(\frac{A \cdot \text{Capacity_Factor}}{\text{Capacity_Factor}(\text{Max_Cap})} + \frac{B \cdot \text{Rated_Power}}{\text{Power}(\text{Max_Cap})} + \frac{C \cdot \text{Pole_Pairs}(\text{Max_Cap})}{\text{Rated_Pole_Pairs}} \right) \cdot \frac{1}{A + B + C} \quad (2.2)$$

Where variables including the Max_Cap are the values calculated for the duration percent correlating to the maximum capacity factor. In this analysis, the values for A, B, and C were set semi-arbitrarily to three, two, and one, respectively. In actual practice, these would be determined by finding the financial cost or profit of an increase or decrease in this variable. The percent duration that produces the largest value of Opt is taken, and the velocity, power, and pole pairs that correlate are chosen.

The results of this first program were output in the form of a tab delimited text file that can be opened in excel. Using the filters in excel, all locations with rated power under 5 kW and

diameters larger than 3 m were filtered out. Next the curve fits and power duration were examined, and USGS 12391950: Clark Fork River below Cabinet Gorge Dam was selected [5]. Figure 2-8 is a photo of this location.



Figure 2-8. Photo of USGS 12391950 [5]

With this site chosen, it was ran through a second MATLAB[®] program. This program is very similar to the first program. The biggest difference is that instead of fixing the diameter, the rated power is set by the user and was set to 10 kW because that was the closest rounded value to that generated in original program. In addition, the optimization constants are changed since rated power is no longer being generated, $A=2$, $B=0$, and $C=1$. This program determined that the rated values for this turbine should be a power of 10 kW, a velocity of 1.67 m/s, an overall diameter of 2.78 m, and 38 pole pairs. It also outputs several useful and interesting figures. The first of these is a plot of velocity duration found in Figure 2-9.

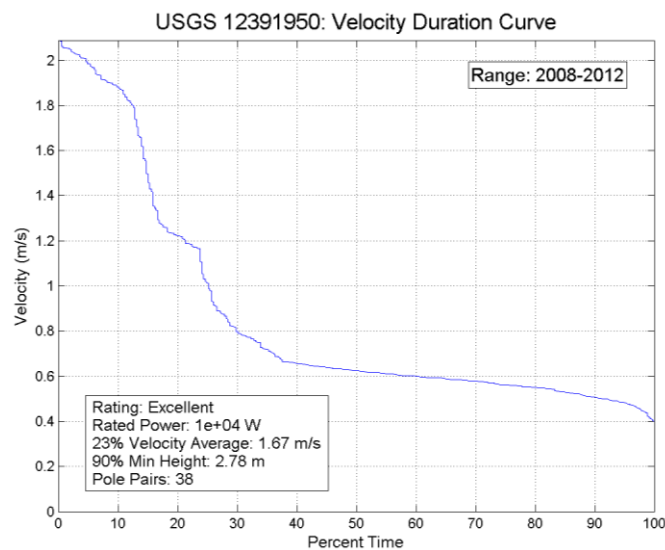


Figure 2-9. Velocity Duration Curve for USGS 12391950

Figure 2-9 shows the velocity of the stream at or above the turbines rated value approximately 12% of the time. Figure 2-10 is a power duration curve for the site.

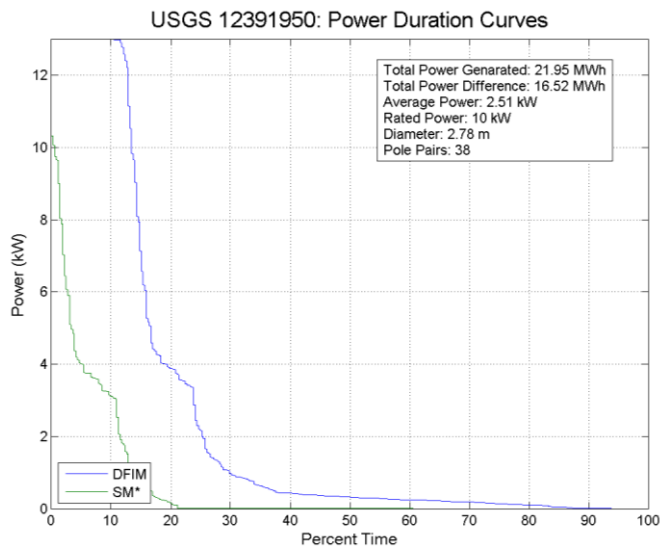


Figure 2-10. Power Duration Curves for USGS 12391950

The SM line is the power duration curve for a permanent magnet fixed speed synchronous generator of the same number of pole pairs connected to the same mechanical turbine design. Figure 2-11 is a similar figure to Figure 1-5 as it presents the daily averages of generation.

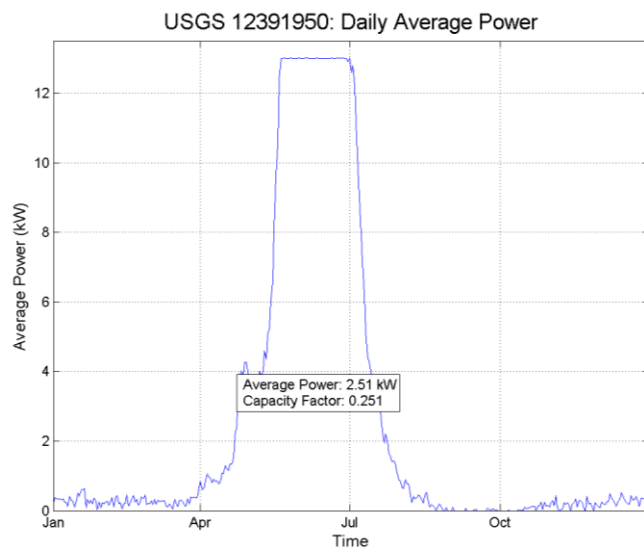


Figure 2-11. Daily Average Power Distribution USGS 12391950

From this plot it is clear that the water turbine does not experience the same problems with variability as wind turbines and produces the majority of its power during the months of May through July.

2.5 SUMMARY

A good understanding of the mechanical portion of the turbine is important for any engineer, electrical or otherwise, planning on working on any component of a hydrokinetic turbine system. This section was meant to inform the reader on several of the options available when designing the mechanical system, as well as, present information on the turbine choice, optimization, and placement for this specific application example. With this background, the next section will focus on the design of the actual electrical machine.

2.6 REFERENCES

- [1] B. Wu et al., *Power Conversion and Control of Wind Energy Systems*. Hoboken, NJ: Wiley-IEEE Press, 2011.
- [2] M.S. Güney and K. Kaygusuz, "Hydrokinetic energy conversion systems: A technology status review," *Renewable and Sustainable Energy Reviews*, vol. 14, no. 9, December, 2010. [Online serial]. Available: ScienceDirect, <http://www.sciencedirect.com/science/article/pii/S1364032110001632>. [Accessed: June 18, 2014].
- [3] M.J. Kahn et al., "Hydrokinetic energy conversion systems and assessment of horizontal and vertical axis turbines for river and tidal applications: A technology status review," *Applied Energy*, vol. 86, no. 10, October, 2009. [Online serial]. Available: ScienceDirect, <http://www.sciencedirect.com/science/article/pii/S0306261909000713>. [Accessed: June 18, 2014].
- [4] R. Radkey, B. Hibbs, and AeroViroment Inc., "Definition of cost effective river turbine designs: final report for the period September 30, 1980 - December 31, 1981," U.S. Department of Energy, Springfield, VA, Tech. Report. December 1981.

- [5] United States Geological Survey, "National Water Information System: Web Interface," *USGS Water Resources*, 2014. [Online]. Available: <http://waterdata.usgs.gov/nwis>. [Accessed: April 4, 2013].

CHAPTER 3: ELECTRIC MACHINE DESIGN

3.1 INTRODUCTION

Although understanding the mechanical system is important, the main focus of this thesis is the design of an appropriate doubly fed induction machine. The purpose of this chapter is to provide the reader an overview of the equations and theory related to the design of an induction machine. This chapter is broken up into four main subsections. The first two sections are more general as they provide background on concepts that would apply to any DFIM. The third section focuses on the design process that was used to design the a DFIM for this hydrokinetic turbine application. The fourth section provides details on the actual machine designed for this application.

3.2 WINDING THEORY

All AC machines are made possible by a sinusoidal varying flux that acts to link the stator and rotor magnetic circuits. The magnetomotive force (MMF), or magnetic potential, acting over the air gap reluctance produces this flux. In order to have a perfectly sinusoidal flux, a perfectly sinusoidal MMF distribution would be required [1]. Unfortunately, this is impossible as the MMF is produced by currents flowing in discrete wires that have been embedded in slots of finite size. Since perfection is still the desired goal, several methods have been developed to make the induced MMF more sinusoidal as well as help improve overall performance of the machine. It is important to be able to examine the MMF function and how successful these efforts were. This is where the winding factors become useful.

In order to understand winding theory and winding factors, Lipo starts by deriving an equation for the magnetomotive force produced in the air gap of a single-phase two pole machine with a single slot per pole and a fully pitched coil. A fully pitched coil is one that spans a full 180 electrical degrees. In Chapter 2 of [1], Lipo steps through this process coming to a result that can be written as (3.1).

$$F_p(\theta) = \sum_h (F_{ph} \cdot \sin(h \cdot \theta)) \quad (3.1)$$

Where h represents harmonics and can be any odd number between one and infinity and F_{ph} is (3.2).

$$F_{ph} = \frac{4}{\pi} \cdot \frac{N_t \cdot I}{2 \cdot h} \quad (3.2)$$

Where N_t is the "total number of turns with which the lines of force are linked", and I is the total current input to the machine [1]. Winding factors were created as a term to scale F_{ph} by, in order to have F_p reflect the changes made by incorporating more advanced winding methods.

The first factor to be addressed here is the pitch factor. This factor arises from the practice of fractional pitched windings, or windings that span less than the full pitch of 180 electrical degrees. According to Lipo "such windings are extensively used for the reason that the MMF waveform is more nearly sinusoidal than with full pitch windings". In addition, fractional pitched coils are shorter and therefore save copper, are stiffer, and will have less resistance [1]. Both references [1] and [2] present equations for the pitch factor, K_{ph} . Equation (3.3) was created by combining parts of each.

$$K_{ph} = \sin\left(\frac{h \cdot p \cdot \pi}{2}\right) \cdot \sin\left(\frac{h \cdot \pi}{2}\right) \quad (3.3)$$

Where p is the winding pitch, which is the ratio of the coil span to a pole pitch [2]. The second sine term is not present in Alger's explanation. Lipo mentions that it is not always included; it acts to make this factor always a positive value.

The next winding factor is the distribution factor, referred to as the winding distribution factor by Alger and the harmonic distribution factor by Lipo. In the simplified machine above, there was only one slot per pole, but this is not the case in most real machines. In order to maximize space utilization, the windings are distributed into several slots. This distribution also acts to remove undesirable harmonics [1]. The formula for the distribution factor, K_{dh} , is listed as (3.4) from [2].

$$K_{dh} = \frac{\sin\left(\frac{h \cdot \pi}{2 \cdot q}\right)}{n \cdot \sin\left(\frac{h \cdot \pi}{2 \cdot n \cdot q}\right)} \quad (3.4)$$

Where "q is the number of phase belts per pole", and n is "the number of slots per phase belt" [2].

The next factor to be considered is the slot opening factor, $K_{\chi h}$. Up to this point, the current of each turn of wire has been assumed to be located at an infinitely small point, but in actuality the current will be distributed across the slot opening. According to Lipo, determining the MMF distribution across a slot precisely would be extremely difficult, but it can be accurately calculated by assuming a linear approximation across the opening [1].

Both [1] and [3] present the formula for this winding factor, although [3] refers to this as the distribution factor because the current is distributed across the slot. Reference [3]'s formula is presented in (3.5), but [1]'s variables are used.

$$K_{\chi h} = \text{sinc}\left(\frac{h \cdot \chi}{2}\right) \quad (3.5)$$

From [3], it can be determined that χ should be the slot opening in electrical degrees, [1] is not very clear on this point.

The last individual winding factor to be covered within this thesis is the skew factor. In a non-skewed stator or rotor, the slots are parallel to the axis of rotation. When the skew is present, the slots are angled by comparison. A typical skew is one or more integer slot pitches. Slot harmonics can be greatly reduced by skewing. Skewing can also help to reduce cogging which is a problem present in squirrel cage machines and any machine with an equal number of stator and rotor slots. In low speed machines, skewing has the added benefit of reducing acoustic noise problems by reducing flux variation at the pole tips [1]. The formula for the skew factor, K_{sh} , is presented in (3.6) in form from [3], but once again using variables from [1].

$$K_{sh} = \text{sinc}\left(\frac{h \cdot \alpha}{2}\right) \quad (3.6)$$

Where

$$\alpha = \text{Skew} \cdot \sigma \quad (3.7)$$

Where Skew is the number of slots between the starting and ending slot and

$$\sigma = \frac{2 \cdot \pi}{\text{Slots}} \cdot P \quad (3.8)$$

In which Slots is the total number of slots in the stator or rotor and P is the total number of pole pairs in the machine.

The product of these four separate winding factors produces the total winding factor K_h . This factor, although developed for the single phase two pole machine, can be used for one phase of a three phase multi pole machine with parallel circuits. Equation (3.9) is used to calculate the MMF of phase a.

$$F_a(\theta) = \frac{8}{\pi} \cdot \left(\frac{N_t \cdot i_a}{C \cdot P} \right) \cdot \sum_h (K_h \cdot \sin(P \cdot h \cdot \theta)) \quad (3.9)$$

Where i_a is the current present in the phase a winding and C is the number of parallel circuits. Equation (3.9) varies slightly from the one presented in [1] as Lipo uses P to denote the total number of poles, but here P denotes the number of pole pairs. This overall winding factor is involved in the calculation of several other usual parameters including mutual inductance.

3.3 EQUIVALENT CIRCUIT PARAMETERS

In order to simplify analysis, steady state equivalent circuits, or lump parameter models, have been developed for most common machines. The DFIM is one machine to have its own equivalent circuit. Figure 3-1 contains the standard steady state equivalent circuit for a doubly fed induction machine.

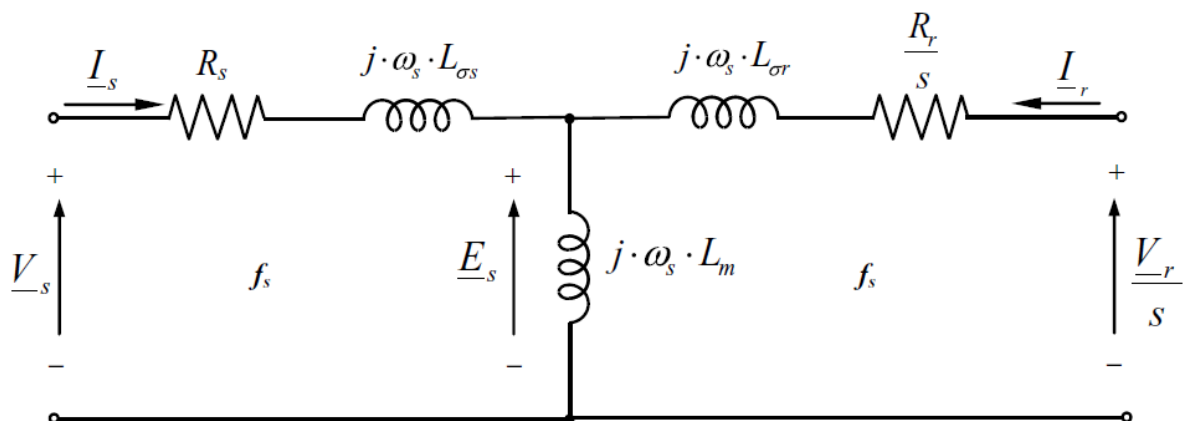


Figure 3-1. DFIM Steady State Equivalent Circuit [4]

The DFIM's equivalent circuit is similar to that of a squirrel cage induction machine with one major difference. In addition to the stator voltage input, there is an input on the rotor side of the circuit as well. The input rotor voltage is divided by the slip of the machine. All the values on the rotor side of the circuit above are reflected to stator side. They are reflected by the u factor which relates the stator and rotor induced EMF at zero speed [4]. The precise relationships between the stator and rotor values can be found in (3.10) through (3.13).

$$R_r = R'_r \cdot u^2 \quad (3.10)$$

$$L_{\sigma r} = L'_{\sigma r} \cdot u^2 \quad (3.11)$$

$$I_r = \frac{I'_r}{u} \quad (3.12)$$

$$V_r = V'_r \cdot u \quad (3.13)$$

Where the variables with the prime symbol such as R'_r are the values referred to the rotor, and the ones without this symbol are the values referred to the stator as used in the equivalent circuit. V'_r would be the actual external voltage applied to the rotor terminals.

The values used in this equivalent circuit can also be used in the simulation model of the DFIM assuming fast transients can be ignored. In order to use the equivalent circuit or simulate the machine, all the resistances and inductances in the circuit above must be calculated.

The first parameters to calculate are the resistances. This can be done using (3.14).

$$R = \frac{L_{\text{turn}} \cdot \rho}{\pi \cdot r_w^2} \cdot \frac{N_t}{C^2} \quad (3.14)$$

Where L_{turn} is the length of a single coil, r_w is the radius of the wire used, and ρ is the resistivity of the desired material scaled to the appropriate temperature. This can be used to calculate both of the actual stator and rotor resistances.

The next parameter to determine is the mutual inductance of the machine. Equation (3.15) contains the overall formula for this inductance taken from [1] with modification.

$$L_m = \frac{3}{2} \cdot \left(\frac{N_e}{2 \cdot P} \right)^2 \cdot \mu_0 \cdot \frac{\pi \cdot r \cdot l_e}{g_e} \quad (3.15)$$

Where μ_0 is the permeability of free space, r is the radius from the axis of rotation to the center of the air gap, and l_e is the effective length of the machine. N_e is the effective number of turns and is calculated using (3.16) from [1].

$$N_e = \frac{4}{\pi} \cdot K_1 \cdot \frac{N_t}{C} \quad (3.16)$$

Where K_1 is the winding factor calculated for the first harmonic, $h=1$. In Equation (3.15), g_e is the effective air gap and is calculated in (3.17) also from [1].

$$g_e = k_c \cdot g \quad (3.17)$$

The variable g is the width of the actual air gap, and k_c is a special multiplier called the Carter Factor which allows for the scaling of the air gap to take into account that the surface of the stator and rotor may have openings for teeth [1]. Reference [1] provides a formula for the Carter Factor that was obtained from conformal mapping and is one of the more accurate ways to calculate this factor. This formula is listed as (3.18).

$$k_c = \frac{\tau}{\tau - \frac{2 \cdot b_o}{\pi} \cdot \left[\text{atan} \left(\frac{b_o}{2 \cdot g} \right) - \frac{g}{b_o} \cdot \ln \left[1 + \left(\frac{b_o}{2 \cdot g} \right)^2 \right] \right]} \quad (3.18)$$

Where τ is the total width of a single tooth and slot, and b_o is the width of just the slot opening. In the case where both the stator and rotor have teeth, a separate Carter factor is calculated for each. They are then multiplied together to produce the factor, k_c , used in (3.17) [1].

There is only one mutual inductance in the equivalent circuit, but it is possible to get two separate values dependent on whether the stator or rotor parameters are used. When this is done, these two values are the mutual inductance reflected to the stator, L_{ms} , and rotor, L_{mr} , respectively. These values can then be used to calculate the value of the u factor. See (3.19).

$$u = \sqrt{\frac{L_{ms}}{L_{mr}}} \quad (3.19)$$

Determining the leakage inductances for the DFIM or any AC machine, is a much more in depth process than anything covered so far. It is so complicated that Lipo dedicated an entire chapter of [1] to just this. Part of this complication is that these leakages are actually the

summation of several different leakage terms. According to the Lipo, there are five major components of leakage flux. These include slot, end winding, harmonic, zig-zag, and skew leakage fluxes; each flux resulting in a component of the overall leakage inductance.

Slot leakage inductance is the result of the flux that passes from one tooth to its neighbor through the slot itself without passing through the air gap to link the other side. Like the overall leakage, the slot leakage for a slot with a double layer winding is made up of multiple components as can be seen in (3.20) from [1].

$$L_{\text{slot}} = L_{1T} + L_{1B} + k_{\text{sl}}(p) \cdot L_{1M} \quad (3.20)$$

Where L_{1T} is the leakage associated with the coils in the top of the slot, L_{1B} is that for the bottom of the slot, L_{1M} is related to the mutual coupling between top and bottom, and k_{sl} is a coil pitch factor that takes into account the fact that, for different values of pitch, some of the slots will have two coils from different phases, where others will have the same phase associated with both coils. The coil pitch factor is a piecewise function that is defined in (3.21), created using information from [1].

$$k_{\text{sl}}(p) = \begin{cases} (3p - 1) & \text{if } \frac{2}{3} < p \leq 1 \\ [3 \cdot (2 \cdot p - 1)] & \text{if } \frac{1}{3} < p \leq \frac{2}{3} \\ (3 \cdot p - 2) & \text{if } 0 < p \leq \frac{1}{3} \end{cases} \quad (3.21)$$

From [1], the equations for the three slot leakage components can be found as (3.22) through (3.24).

$$L_{1T} = 3 \cdot \left(\frac{N_t}{C} \right)^2 \cdot l_e \cdot \frac{\rho_T}{\text{Slots}} \quad (3.22)$$

$$L_{1B} = 3 \cdot \left(\frac{N_t}{C} \right)^2 \cdot l_e \cdot \frac{\rho_B}{\text{Slots}} \quad (3.23)$$

$$L_{1M} = 3 \cdot \left(\frac{N_t}{C} \right)^2 \cdot l_e \cdot \frac{\rho_{TB}}{\text{Slots}} \quad (3.24)$$

The variables ρ_T , ρ_B , and ρ_{TB} are the specific slot permeances and are related to the geometry of the slot. A generic geometry for a slot containing a double layer winding can be found in Figure 3-2 on the next page.

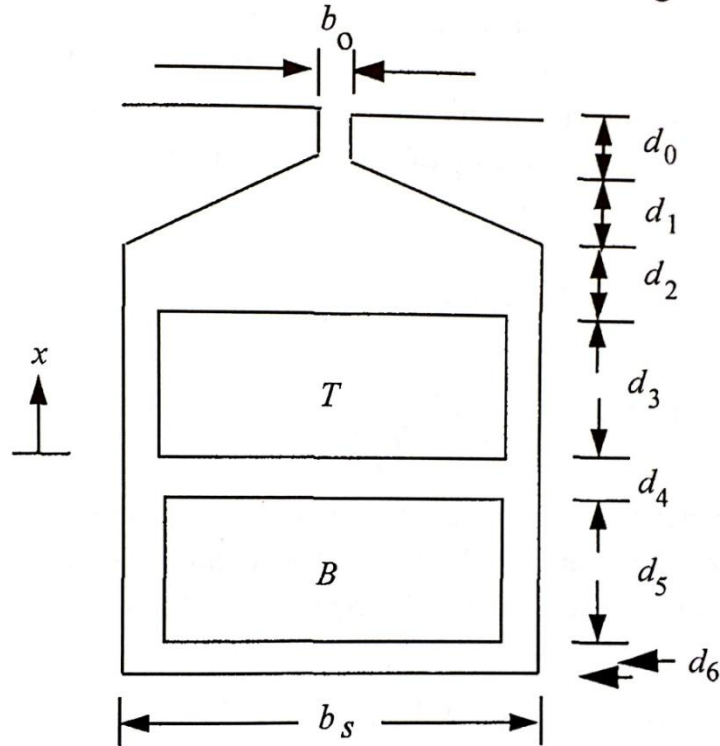


Figure 3-2. Generic Slot Geometry with Double Layer Winding [1]

If the fact that each layer of the winding is made up of multiple conductors with insulation and maybe even some air between is ignored and each winding is approximated as a single square shape conductor, the specific permeance equations become:

$$\rho_T = \mu_0 \left(\frac{d_3}{3 \cdot b_s} + \frac{d_2}{b_s} + \frac{d_1}{b_s - b_o} \cdot \ln \left(\frac{b_s}{b_o} \right) + \frac{d_0}{b_o} \right) \quad (3.25)$$

$$\rho_B = \mu_0 \left(\frac{d_5}{3 \cdot b_s} + \frac{d_2 + d_3 + d_4}{b_s} + \frac{d_1}{b_s - b_o} \cdot \ln \left(\frac{b_s}{b_o} \right) + \frac{d_0}{b_o} \right) \quad (3.26)$$

$$\rho_{TB} = \mu_0 \left(\frac{d_0}{b_o} + \frac{d_1}{b_s - b_o} \cdot \ln \left(\frac{b_s}{b_o} \right) + \frac{d_2}{b_s} + \frac{d_3}{2b_s} \right) \quad (3.27)$$

The next component of leakage inductance is from the end winding leakage flux. "The overhang or end winding portion of a winding produces a distinctly different component of leakage flux whose magnetic circuit is almost entirely in air" [1]. This leakage can be significant in machines with a low number of poles; for example in a 4 pole machine, end winding leakage is approximately 49-68% of the total leakage inductance. The more poles in the machine, the smaller this percent becomes [1]. For a 38 pole pair, 76 pole, machine, this leakage may even be negligible, but it will still be included for completeness and accuracy.

In actuality, these inductances are created by image currents being created in the surface of the iron. The main equation for end winding leakage is shown as (3.28).

$$L_{ew} = \frac{1}{P} \cdot K_{d1}^2 \cdot K_{p1}^2 \cdot \left(\frac{N_t}{C}\right)^2 \cdot L_{ew1} \quad (3.28)$$

Where L_{ew1} is the inductance of the end winding of a single turn of the coil. Lipo shows two methods for calculating this value; one method treats the iron as a perfect conductor and the other treats it as air. Neither of these methods will produce the correct value, but experimental evidence suggests that the value should be about halfway in between, and, therefore, the results from these two methods can be averaged to produce a good approximation. The L_{ew1} can be calculated using the perfect conductor method, using (3.29).

$$L_{ew1_pc} = \frac{\mu_0}{\pi} \cdot \left[\begin{aligned} & -2a \cdot \ln \left[\frac{2a}{b} + \sqrt{\left(\frac{2a}{b}\right)^2 + 1} \right] - b \cdot \ln \left[\frac{b}{2a} + \sqrt{\left(\frac{b}{2a}\right)^2 + 1} \right] \dots \\ & + 2a \cdot \ln \left(\frac{4a}{\varepsilon} \right) + b \cdot \ln \left(\frac{2 \cdot b}{\varepsilon} \right) + 2 \cdot \sqrt{4a^2 + b^2} - 2 \cdot b - 4a \end{aligned} \right] \quad (3.29)$$

Where ε is the radius of the conductor, a is the distance from the surface to the center of the coil, and b is the total distance spanned by the coil. In order for (3.29) to be valid, b must be much greater than ε [1].

Equation (3.30) is the formula required to calculate L_{ew1} when the iron is treated as air.

$$L_{ew1_a} = \frac{\mu_0}{2 \cdot \pi} \cdot \left[\begin{aligned} & -2 \cdot \sqrt{a^2 + b^2} + 3 \cdot \sqrt{4a^2 + b^2} - 4a - b + 2a \cdot \ln \left[\frac{2 \cdot (a + \sqrt{a^2 + b^2})}{b} \right] \dots \\ & + -4a \cdot \ln \left(\frac{2a + \sqrt{4a^2 + b^2}}{2b} \right) + 2a \cdot \ln \left(\frac{\varepsilon}{b} \right) + 2a \cdot \ln \left(\frac{4a}{\varepsilon} \right) \dots \\ & + -b \cdot \ln \left[\frac{b}{2a} + \sqrt{\left(\frac{b}{2a}\right)^2 + 1} \right] + b \cdot \ln \left[\frac{b}{\varepsilon} + \sqrt{\left(\frac{b}{\varepsilon}\right)^2 + 1} \right] \end{aligned} \right] \quad (3.30)$$

Variables used in (3.30) are the same as those used in (3.29).

Another source of leakage is the harmonic leakage, sometimes referred to as the belt leakage. This component arises because the flux produced in the machine is not a perfect sine wave, but has harmonics other than the fundamental present. Since the fundamental component is the only source of useful power transfer, these additional harmonics must be accounted for in a loss term [1]. Equation (3.31) can be used to calculate this leakage.

$$L_{lk} = L_m \cdot \left[\frac{1}{K_1^2} \cdot \sum_{h=2}^{\infty} \left(\frac{K_h}{h} \right)^2 \right] \quad (3.31)$$

There is a component of flux that travels back and forth, or zig-zags, between the surface of the stator and rotor teeth. "This flux depends upon the length of the air gap and the relative instantaneous positions of the tooth tips" [1]. Equation (3.32) shows the zig-zag leakage inductance for a two layer winding taken from [1].

$$L_{zz} = \begin{cases} \left[\frac{3}{\text{Slots}} \cdot \left(\frac{N_t}{C} \right)^2 \cdot l_e \cdot \frac{(2lp - 5)}{4} \cdot \rho_{zz} \right] & \text{if } \frac{2}{3} < p \leq 1 \\ \left[\frac{27}{4} \cdot \left(\frac{N_t}{C} \right)^2 \cdot \frac{l_e}{\text{Slots}} \cdot \rho_{zz} \right] & \text{if } \frac{1}{3} < p \leq \frac{2}{3} \\ \left[3 \cdot \left(\frac{N_t}{C} \right)^2 \cdot \frac{l_e}{\text{Slots}} \cdot \frac{27p}{4} \cdot \rho_{zz} \right] & \text{if } 0 < p \leq \frac{1}{3} \end{cases} \quad (3.32)$$

The variable ρ_{zz} is the specific permeance related to this inductance and is dependent on the width of the stator and rotor teeth, t_{os} and t_{or} respectively, as seen in (3.33).

$$\rho_{zz} = \frac{\mu_0 \cdot t_{os} \cdot t_{or} \cdot (t_{os}^2 + t_{or}^2)}{6 \cdot g_e \cdot \tau^3} \quad (3.33)$$

Although skewing the stator or rotor offers many benefits, the downside is that it decreases the amount of flux that actually couples the stator and rotor. This decrease in coupling can be modeled as an increase in leakage. This leakage component is calculated using (3.34) [1].

$$L_{lsk} = L_m \cdot \frac{1 - K_{s1}^2}{K_{s1}} \quad (3.34)$$

As mentioned earlier, the total leakage per phase is a summation of all five leakage components as seen in (3.35).

$$L_l = L_{slot} + L_{ew} + L_{lk} + L_{lzz} + L_{lskr} \quad (3.35)$$

This method to calculate the leakage can be used for both the stator and rotor values assuming appropriate values are used. The rotor leakage calculated will be relative to the rotor and, therefore, will need to be adjusted using (3.11) for use in the equivalent circuit.

3.4 THE DESIGN PROCESS

The large number of poles desired for this gearless geometry creates a complication, as the circumference of the machine must be large enough to have at least three slots per pole. This means that the machine may be too large for conventional placement inside the nacelle at the center of the turbine. To accommodate the larger diameter, the machine will be incorporated into the first ring of the duct so that the rotor of the machine and the blade assembly are essentially one piece. This is shown in Figure 3-3.

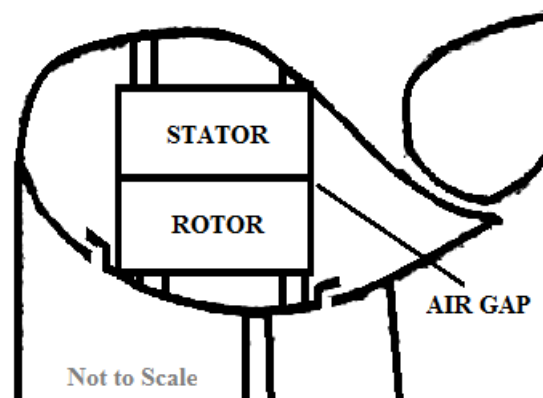


Figure 3-3. DFIM Geometry within Duct Ring

This new geometry creates several constraints in the design of this DFIM. From careful measurements, the axial length of the machine is limited to 0.242 m, the air gap must be at a radius of 1.016 m, and the rotor and stator iron are each limited to a thickness of 80.645 mm for a standard 10ft diameter turbine assembly. For the 2.78 m diameter model being designed here, these values are 0.221 m, 0.927 m, and 73.554 mm respectively.

In addition, there are several other constraints placed on the design to align with convention, preference, and/or other external constraints. In this design, the rated power was set with reference to the mechanical portion of the system and was therefore set using the 10 kW mechanical system rating. The rated voltage for the DFIM was set at 480 V RMS line to line. This voltage was chosen because it is a standard rating for low power distributed generation. Since this turbine will be located in the United States and grid connectivity was a requirement, the rated frequency was set as the standard 60 Hz. For a three phase machine, there is a choice of whether to wind it to have 1.5 phases per pole or three phases per pole.

Three was chosen because it helps decrease losses and is more commonly used by convention. To simplify analysis, parallel circuits were not used.

From reading [2] by Alger, there are several useful rules of thumb (ROTs) that can be applied to help create other constraints. Alger says that the pitch of the machine should be as close to 5/6 as possible as this value will result in much lower harmonics and a much cleaner sine wave for flux as it zeroes out the triplen harmonics. Another ROT can be found as (3.36).

$$\frac{2 \cdot P \cdot g}{\pi \cdot D} \leq .01 \quad (3.36)$$

If the difficulty and expense in creating an extremely small air gap is taken into account, then it can be seen that the desired air gap would be the largest possible that still meets this criteria, which results in (3.37) as an additional constraint.

$$g = \frac{.01 \cdot \pi \cdot D}{2P} \quad (3.37)$$

It may be impossible to have an air gap as small as desired due to construction constraints, in this case, use the smallest gap possible. An additional ROT from Alger is that b_o , the slot opening, should be at most 54% of τ , the total slot and tooth width combined.

A basic approach for designing the stator of the machine can be derived from reading Alger. This approach is based on neglecting everything but the magnetizing branch of the steady state circuit of the induction machine. When this is done, two main design equations fall out: (3.38) and (3.39).

$$E = \frac{2 \cdot \pi \cdot f_s \cdot K_1 \cdot N_t \cdot \sqrt{3} \cdot \Phi_M}{\sqrt{2} \cdot C} \quad (3.38)$$

$$I = \frac{\sqrt{2} \cdot P^2 \cdot g_e \cdot \Phi_M \cdot \pi \cdot C}{2 \cdot \mu_0 \cdot q \cdot N_t \cdot K_1 \cdot D \cdot l_e} \quad (3.39)$$

There are some differences between the presentation of these equations here and in [2]. Here voltage, E , is the desired rated voltage in RMS line to line, where in Alger's text it is a line to neutral value, therefore, a root three term has been added. In Alger's formulas, he only took into account the pitch and distribution factors, but here the total winding factor is used. These equations were also modified so they can be used with parallel circuits, should the

reader desire to do so. In this design process, the voltage multiplied by current must equal the desired rated power, within tolerance, while varying other parameters.

It was very hard to find a good text to explain design of the rotor of DFIM. After much thought, it was decided to use the same approach that was used for the stator. The main differences being that the desired rated power and speed were both set to be 30% of the stator rated values. In addition, flux was constrained to be equal to that of the stator since they must be magnetically coupled.

The actual approach used was to vary the gauge of wire used in the stator and rotor, as well as the number of turns in each. For each iteration, certain criteria were examined, and if any were not met, that iteration was discarded. Rotor voltage must be less than the stator voltage. Both stator and rotor rated powers must be within +10% of their desired values. The gauge of wire being used for the stator and rotor must have a current carrying capacity greater than the rated currents. Both leakage terms must be less than 15% of the mutual inductance. Finally, the losses for each iteration were examined, and the iteration with the lowest losses was chosen. The values of diameter and current carrying capacity for each wire gauge was taken from Reference [5]. The Mathcad sheet used to design the DFIM used in the thesis is located in Appendix A.

3.5 THE ACTUAL DESIGN

The full design of this DFIM can be found in Appendix A. Some highlights of the machine are included in this section. Both the stator and rotor of this machine have 456 slots with a perfect $5/6$ pitch. The stator of the machine is skewed two slots to avoid cogging. The wire gauges required for the machine are 8 AWG and 2 AWG for the stator and rotor respectively. These gauges are a little large for a typical machine and may be difficult to bend, namely the two gauge. This problem could be circumvented if the design was redone to allow parallel windings or stranded conductors. This machine requires 608 series turns on the stator and 380 on the rotor.

The equivalent circuit parameters for this DFIM are as follows. The resistances for the machine are 0.877Ω for the stator and 0.32Ω for the rotor when reflected to the stator. The

mutual inductance for the DFIM is 58.243 mH. The u factor is 1.528. The leakages are 7.509 mH, for the stator leakage inductance, and 4.924 mH, for the rotor reflected to the stator.

When the rotor terminals of this machine are shorted together and rated voltage is applied, Figure 3-4's power vs. speed curve can be produced. With the rotor terminals still shorted, a slip of -0.017 would be required to generate the desired rated power of 10 kW. At this operating point, the power factor would only be 0.59. When running a DFIM there is complete control of the power factor. In fact unity power factor can be produced if desired.

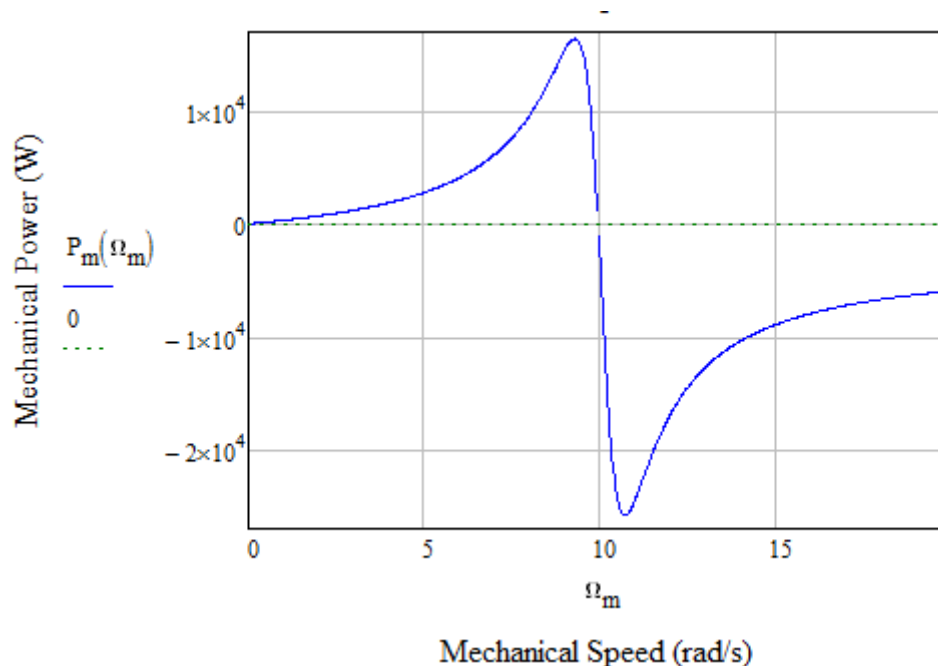


Figure 3-4. Power vs. Speed Curve for Designed DFIM with Shorted Rotor

3.6 SUMMARY

This chapter acted as a means to convey the basic knowledge required to understand the design of any AC machine, such as winding theory and calculation of the equivalent circuit parameters including resistances and inductances. Next, it went through the design approach used in this thesis for the creation of a DFIM that would be adequate for this specific hydrokinetic turbine application. Finally, the highlights of this finished design were covered. Now that the mechanical system and the design of the electric machine have been discussed, the next chapter of this thesis will cover the simulation of the whole system as well as a scheme to control it all.

3.7 REFERENCES

- [1] T.A. Lipo, *Introduction to AC Machine Design*, 3rd ed. Madison, WI: Wisconsin Power Electronics Research Center: University of Wisconsin, 2011.
- [2] P.L. Alger, *Induction Machines*, 2nd ed. New York, NY: Gordon and Breach Science Publishers, 1970.
- [3] J. Law, "Multiple Circuit Winding Example Solution (xmcd)," class notes for ECE 520, Department of Electrical and Computer Engineering, University of Idaho, 2013. [Online]. Available: <http://www.ee.uidaho.edu/ee/power/jlaw/COURSES/ECE520/F13/Midterm/P1Solution.xmcd>. [Accessed: June 24, 2014].
- [4] G. Abad et al., *Doubly Fed Induction Machine: Modeling and Control for Wind Energy Generation Applications*. Hoboken, NJ: Wiley-IEEE Press, 2011.
- [5] C.R. Nave, "Electrical Wire Gauges," *HyperPhysics*, 2012. [Online]. Available: <http://hyperphysics.phy-astr.gsu.edu/hbase/tables/wirega.html>. [Accessed: June 25, 2014].

CHAPTER 4: SIMULATION AND CONTROL

4.1 INTRODUCTION

An original goal for this thesis was to construct the actual machine in order to perform operational tests. Unfortunately, this quickly became infeasible due to cost and time constraints. The next best option was to use simulation to demonstrate proper operation. To do this, a model of the machine and its supporting systems was constructed using Simulink[®]. The complete system was modeled from the velocity input right up to the terminals of the transformer as seen back in Figure 1-9, minus the gearbox, as there is not one in this application. Nearly idealized models were used for the turbine, mechanical coupling, and voltage source converters, where the actual machine and controllers were much more precise. This section is broken up into three main sections. The first section will cover the modeling of the main electrical components such as the DFIM and rotor side converter. The second section focuses on the two main mechanical systems, the turbine itself and the mechanical coupling. The third section will cover the controls implemented on these systems. Even though the Simulink[®] model contains the grid side converter, DC Bus, and their controllers, they will not be discussed here as they are not the main focus of the thesis. They were designed using techniques from [1] as well as material covered in *ECE 504: T&D Applications of Voltage Source Converters* at the University of Idaho in Spring 2013.

4.2 ELECTRICAL SYSTEM MODELS

The first system presented here, the most important, is the doubly fed induction machine itself. There are several dynamic models for an induction machine, each with various differences. One common point of difference is the choice of reference frame. For a three phase machine, most would think to create a model that uses phase currents, but there are methods that can be used to change the reference frame so that, for an ungrounded system, there are only two currents used in the model. In this case, these currents will have a 90 degree phase difference and can have different magnitudes. When this is done, there is a choice of whether to have a stationary or rotating reference frame. When the reference frame is stationary, the two currents produced will still be oscillating at the same frequency as the phase currents. When the reference frame is rotating, the frequency of these currents will be

different from the abc currents; they can even be DC in steady state for a synchronous reference frame. A stationary reference was selected for the model used for this application. The stationary reference frame is usually referred to as an $\alpha\beta$ reference frame, with one current being α and the other β . Another difference arises from the choice of whether β leads or lags α . In the model used β leads by 90 degrees [2]. Information on performing reference transformations can be found from a variety of sources including Appendix A of [2]. Another difference is whether to use current or flux as the state variable. Although flux will be slightly more accurate, it is often more convenient to use the currents. The model used in this thesis is presented in Figure 4.1, on the following page, taken from [2] with modifications to reflect what was actually used.

In this model of the DFIM:

$$L_s = L_{ls} + L_{lr} \quad (4.1)$$

$$L_r = L_{lr} + L_m \quad (4.2)$$

$$\sigma = 1 - \frac{L_m^2}{L_s \cdot L_r} \quad (4.3)$$

The other important electrical component is the switching model. The most common voltage source converter used in this application is the two level VSC. There are several different models for this converter, each with different levels of complexity. There is one model that is extremely idealized and uses functions to produce perfect sine waves. The next level of complexity up uses ideal switches so that the harmonics can be observed, but losses are neglected. After that, there are a multitude of models taking losses into account in different ways. The second level of complexity was chosen here. The topology of the ideal switching model is presented in Figure 4-2 where S_A , S_B , and S_C are the states of the switching functions.

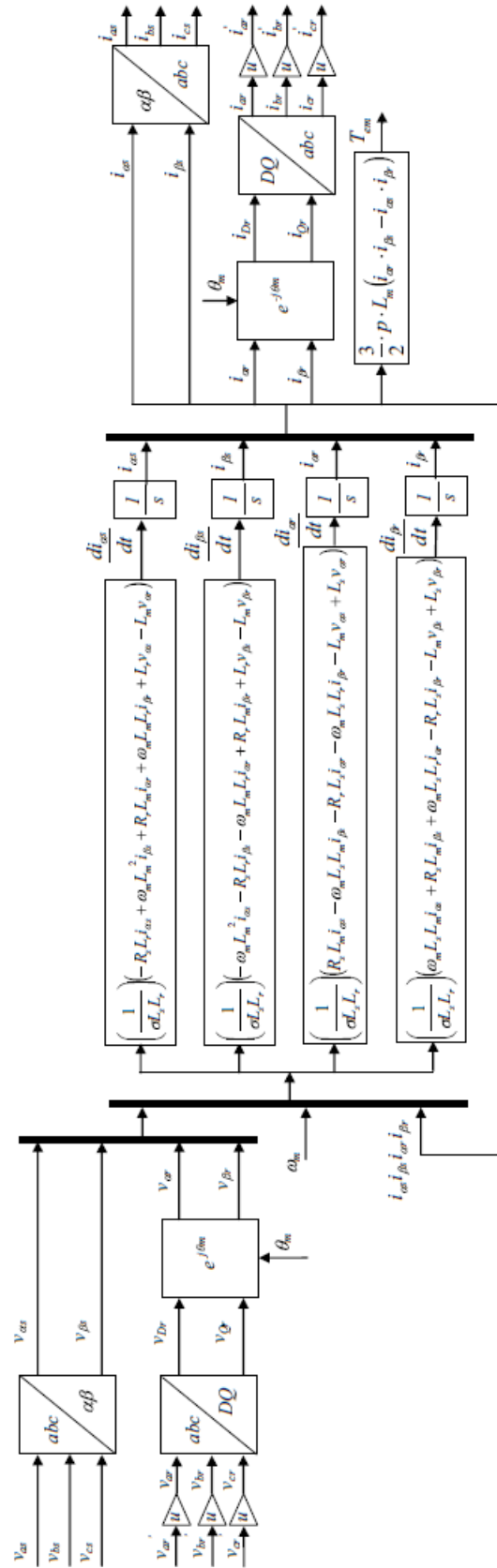


Figure 4-1. Simulation Block Diagram of DFIM Dynamic Model [2]

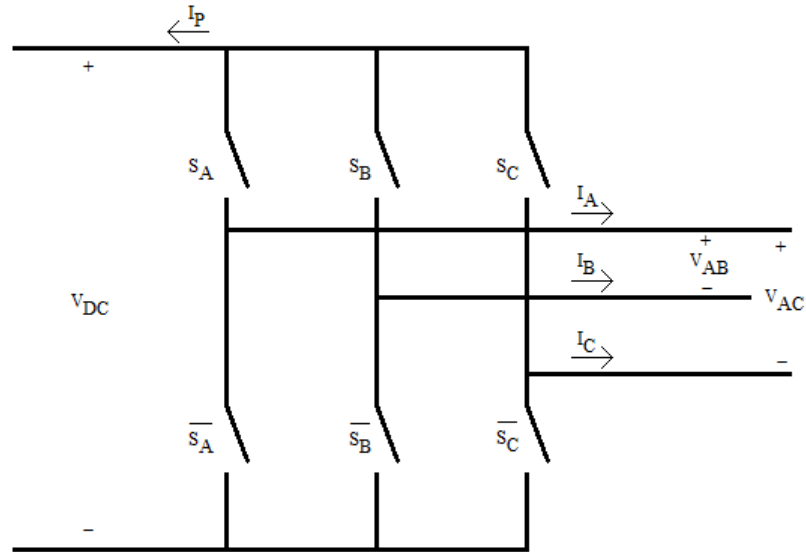


Figure 4-2. Topology for Ideal Switching Model of Two Level VSC

Reference [1] and ECE 504 present a very similar model for the ideal switching model. In both models, there is an assumption that the DC Bus is constructed with a neutral point between two equal sized capacitors. Therefore, there are both positive and negative DC voltage available. Without connecting a neutral wire between the machine and this neutral point this is not possible. It appears, from most texts, that this DC Bus is usually a single capacitor bank, therefore, there is no negative value available. During simulation, the switching model broke down. A new switching model was derived after extensive discussion with Dr. Herbert Hess. This model is summed up in the following six equations.

$$V_{AB} = (s_A - s_B) \cdot V_{BUS} \quad (4.4)$$

$$V_{AC} = (s_B - s_C) \cdot V_{BUS} \quad (4.5)$$

$$V_A = \frac{1}{3} \cdot (2 \cdot V_{AB} + V_{AC}) \quad (4.6)$$

$$V_B = \frac{1}{3} \cdot (-V_{AB} + V_{AC}) \quad (4.7)$$

$$V_C = \frac{1}{3} \cdot (-V_{AB} - 2 \cdot V_{AC}) \quad (4.8)$$

$$I_P = -(s_A \cdot I_A + s_B \cdot I_B + s_C \cdot I_C) \quad (4.9)$$

4.3 MECHANICAL SYSTEM MODELS

There are two main mechanical components that needed to be modeled. The first of these was the actual turbine. The inputs to this model were the water and rotational speeds; the output was a torque. For simplicity, the method derived for the actuator disk theory was used. Using the two input speeds, the model uses (2.1) to calculate an appropriate tip speed ratio. The effective power coefficient was then determined using the relationship approximation from Chapter 2. The velocity of the water and the power coefficient were then entered into (1.2) to produce the mechanical power; where A_0 is the total duct area. This mechanical power was then divided by the rotational speed to produce torque and multiplied by negative one to line up with the motor convention of the DFIM. This torque is the T_{load} used in the next system.

The other mechanical model is for the coupling between the electrical machine and the water turbine. This model takes in a torque input from each of these source and uses them to produce the rotational speed for the system. An extremely simplified model was chosen as per [2]. In this model there is only a single inertia for both systems. For most applications, this is not accurate as the turbine and electrical machine are separate from each other coupled by a shaft and sometimes a gearbox. In this application, this model may be more accurate as the turbine blades are directly connected to the rotor of the machine. This model is summed up by (4.10) taken directly from [2].

$$T_{em} - T_{load} = J \cdot \left(\frac{d}{dt} \Omega_m \right) \quad (4.10)$$

Where T_{em} is the electromagnetic torque produced by the DFIM, T_{load} is the torque consumed by the mechanical turbine, J is the inertia of the machine, and Ω_m is the mechanical rotational speed. The units for torque are $N \cdot m$, inertia is $kg \cdot m^2$, and rotational speed is rad/s .

An approximate inertia for this machine was determined using (4.11) taken from [3].

$$J = \frac{1}{2} \cdot M \cdot (a^2 + b^2) \quad (4.11)$$

This is the moment of inertia of a hollow cylinder where M is the mass of the cylinder, a is its internal radius, and b is its external radius. To calculate total inertia, J was calculated for

a ring of solid copper with an outer radius equal to the radius of the rotor and an internal radius decreased by the slot depth. Another J was calculated for a iron ring with an outer radius equal to the copper ring's inner radius and an inner radius equal the inner radius of the rotor. There two separate inertias were added together to get an approximate total of 600 kg*m².

4.4 CONTROLS

Now with a basic understanding of the system models, it is possible to go through the controls process. The first controller measures the velocity of the water in the stream and determines an appropriate desired rotational speed. This controller was designed so that, under idealized conditions, the real power through the rotor would be at most 30% of the mechanical power rating and stator power would be at most 160% of this rating. Some would question allowing 160% on the stator. This can be allowed because the machine is designed with the ability to handle the current when the machine's rotor terminals are shorted together. Under this condition, the machine presented in Chapter 3 has an apparent power rating of about 16 kVA. With the DFIM, there is the ability to control the reactive power to stay at any value including zero, therefore, we can get to 160% rated power without exceeding the apparent power rating. In addition, during the time when the stator has the large output power, the rotor is absorbing approximately 30% of the power, so the transformer still only sees the 130% rated power.

At first glance this controller seems like it would be rather simple. Since maximum power capture is desired, it would make sense to determine the desired rotation speed using (4.12).

$$f_m = \frac{X_{Cpe_Max} \cdot V}{\pi \cdot D} \quad (4.12)$$

Where f_m is the rotational speed in Hz, X_{Cpe_Max} is the tip speed ratio that produces the maximum power coefficient, and D is the diameter of the blades. Unfortunately, there are constraints on the operation of the DFIM that keep this from always being possible. As a result of these limits, there are actually three or four operation ranges depending on how the third operation range is handled. The lowest rotational speed allowed by the DFIM is 70% of the rated value. As a result, the speed produced by (4.12) will not be possible to match up to a certain velocity, approximately 1.16 m/s for this application. In this first operating

region, rotational speed should be held at 70% of rated. Doing so will produce the largest power coefficient possible and, therefore, the maximum power capture. In the next region, (4.12) is fully valid. The problem here is that at a specific velocity, about 1.83 m/s here, the power produced with this rotational speed would exceed the 130% maximum value. At this point, it is desired to start decreasing the rotational speed to create a tip speed ratio that will result in a lower power coefficient that will still produce 130% rated power. The limit in this section is that as the speed begins to decrease, the amount of power going through the rotor will increase, and this value needs to not exceed approximately 30% rated. Reference [2] presents an approximate relationship between the mechanical power, P_m , and the stator power, P_s , shown in (4.13).

$$P_m = (1 - s) \cdot P_s \quad (4.13)$$

Where s is slip. From this relationship, another can be derived between rotor power, P_r , and mechanical power.

$$P_r = \frac{f_r - f_m}{f_m} \cdot P_{mec} \quad (4.14)$$

Where f_r is the rated mechanical rotational speed in Hz. In order to meet the constraints, the minimum allowable rotational speed in this region is 81.3% of rated instead of 70%, as in the first region.

In this region, the desired mechanical speed is calculated through an iterative approach. First the maximum possible tip speed ratio is calculated using (2.1) with a rotational speed 130% rated. If this number is larger than X_Cpe_Max , then it is set as this value instead. Next, the minimum ratio is calculated using the minimum allowable rotational speed. It is then possible using (1.2) to calculate a desired power coefficient. The tip speed ratio that produces the desired power coefficient within the bounds is determined through iteration. This tip speed ratio is then used to determine the desired rotational speed.

Depending on the method used for iteration, it may be necessary to have a fourth region, or more accurately, an operating point. Some methods will not find the case where the correct tip speed ratio is the minimum allowable. In the Simulink® model, all four possible

rotational speeds are calculated, but only one is selected based on logic operations. This rotational speed is then converted into radians per second.

With the desired rotational speed determined, another controller is designed as an outer loop controller to force the system to reach and maintain the desired speed. This controller uses the desired and actual rotational speeds as inputs and outputs a desired torque for the DFIM. For simplicity and time, a simple PI controller was implemented as seen in Figure 4-3.

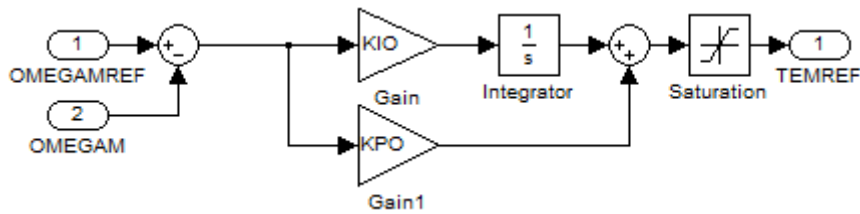


Figure 4-3. Simulink[®] Model of Rotational Speed Controller

The gains in this model were determined using the following equations.

$$TIO = 2 \cdot TIR \quad (4.15)$$

$$KIO = \frac{1}{TIO} \quad (4.16)$$

$$KPO = \frac{J}{TIO} \quad (4.17)$$

Where TIR is the time constant from the inner current controller that will be discussed next. TIO is the time constant for this controller. The saturation block was added to this model to prevent the controller from "throwing lightning bolts." For large differences in rotational speed inputs, the large gains could cause the controller to demand torques that the machine cannot produce and would damage it. The saturation block acts to limit the desired torque within a safe region. This was set with an upper limit of positive 1 pu and negative 2.5 pu torque. Although this controller performs its intended function, it is by no means the best solution and was rushed due to time constraints. Although a simple PI controller may seem like a good solution, according to Dr. Richard Wells, an Emeritus Professor at the University of Idaho, it is rarely the best.

The remaining controllers are more focused on controlling the electrical system. In these models the dq reference frame is used. The dq reference frame is a synchronous rotating

reference frame where q leads d by 90 degrees. In this reference frame, values oscillating at synchronous frequency will become DC quantities. The reference angle is determined using a phase lock loop (PLL) which is designed to align with the stator voltage so that the d axis is equal to the magnitude of the three phase wave and the q value is zero. Reference [1] provides an extensive reference on the design of the PLL.

The next controller takes the desired torque reference and a reactive power reference and produces desired dq currents. The biggest benefit of using this dq reference frame is that it effectively decouples these two input quantities. Torque becomes directly dependent on d axis current, and reactive power becomes directly dependent on q axis current. The controller used here is based on the formulas presented in Chapter 8 of [4], but was modeled in a structure similar to the presentation in [2]. A Simulink[®] block diagram of the current reference calculator is presented in Figure 4-4.

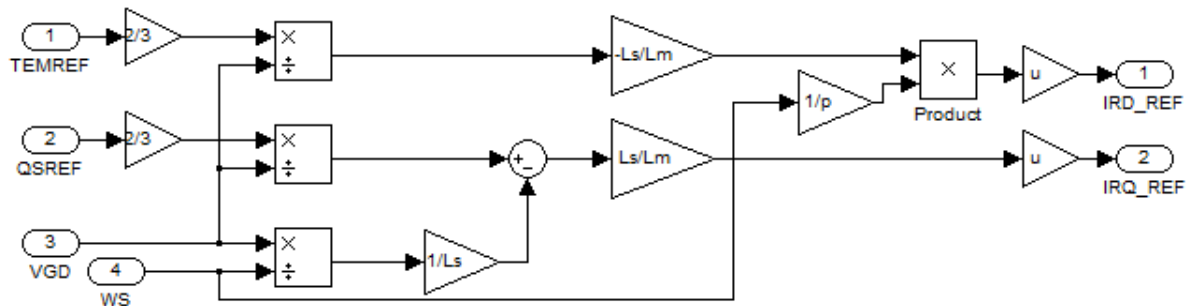


Figure 4-4. Simulink[®] Model of Current Reference Calculator

In this model, p is the number of pole pairs, previously defined as P . VGD is the d -axis value of grid, or stator, voltage. WS is the synchronous frequency also determined by the phase lock loop.

The next controller is the current control loop which uses a combination of feedback and feed-forward compensation to force the actual dq currents to match their references. The exact controller used in this application was primarily based on the one presented in [2], but was also affected by one in [1] as well as concepts learned in ECE 504. A block diagram of current control loop for the rotor side converter is presented in Figure 4-5 on the following page.

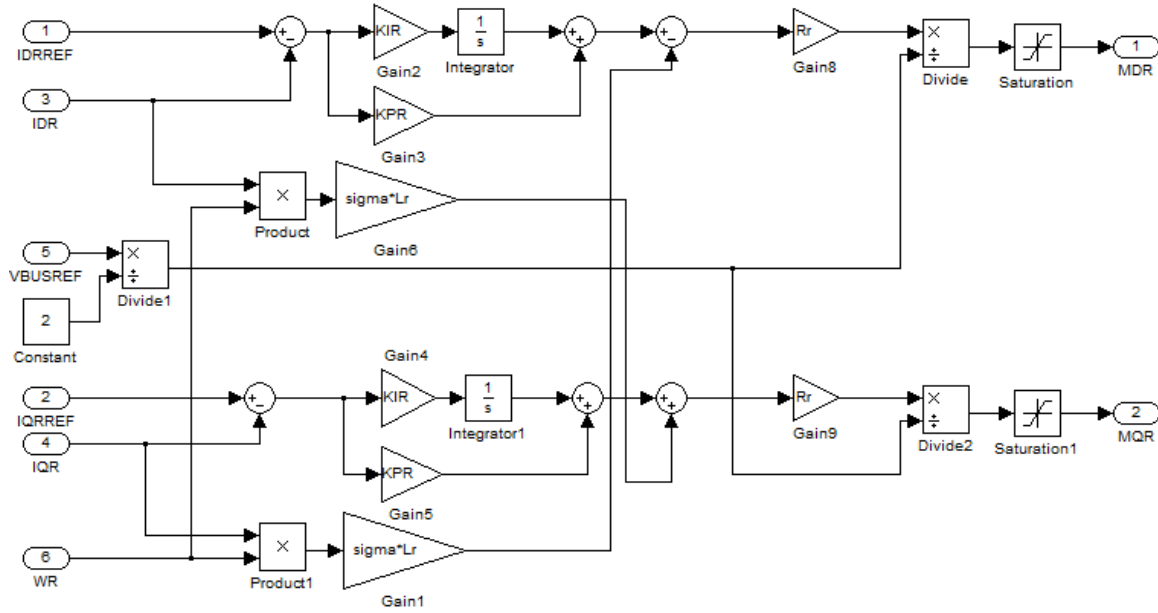


Figure 4-5. Simulink[®] Model for the Current Control Loop

In this model sigma is another variable for σ . The gain constants were set using the formulas presented in [1].

$$KPR = \frac{\sigma \cdot \tau_r}{\tau_{ir}} \quad (4.18)$$

$$KIR = \frac{1}{\tau_{ir}} \quad (4.19)$$

$$\tau_r = \frac{L_r}{R_r} \quad (4.20)$$

The variable τ_{ir} is a design parameter which was set to twice the inverse of the switching frequency in rad/s. The two outputs of this controller will be converted into the ABC domain and then used with sine triangle pulse width modulation to produce the switching commands. In ECE 504, Dr. Johnson taught that these outputs must be within the bounds of minus to positive one in order to avoid over modulation, and, therefore, limiters are needed before the outputs.

As mentioned in the introduction, the model used for simulation was more complex, in that it contained a model of the DC bus as well as the switches and control used to maintain the bus voltage. These were omitted here because they are not really inside the scope of this thesis. The DC bus voltage was controlled to a value of 1000 V.

4.5 SIMULATION RESULTS

The original plan for the simulation was to show how the model reacts to actual changes within the stream of interest. Unfortunately, data was only available in 15 minute intervals and would have taken too much computing time to properly simulate. Instead, a simulation was done in which the system locked into an initial value and then experienced a significant step change in input.

This simulation shows the start up of the machine. The approach used is probably not the best for an actual application, but was able to allow for accurate simulation with limited difficulty. For the first half second of simulation, the turbine is not allowed to spin, and no electrical components are active besides the phase lock loop which is attempting to lock in. After this half second mark, the grid side converter brings the DC bus up to rated voltage and the turbine is allowed to spin. At this point, neither the stator or rotor of the machine is connected, so the turbine is only being sped up by the power being produced by the 2.2 m/s velocity of the water. Even though the machine is not connected, the controller is already calculating the desired rotational speed based on the input velocity. When this speed is surpassed by the system, both stator and rotor terminals of the machine are connected simultaneously. This produces a significant transient that could be avoided if the rotor was connected first and the stator voltage was synchronized with the grid before connection. This improvement was not made due to time constraints and the fact that control is not the primary focus of this thesis. With the system fully active, the controller forces the machine to generate the desired power. At four seconds, the velocity of the water decreases instantly to 1.9 m/s and the desired rotational speed increases in order to maintain maximum power generation.

On the next page, Figure 4-6 shows a comparison between the desired and actual mechanical rotational speeds over the course of the simulation. From the curve, it can be seen that the machine is connected at about 2.2 s. In this simulation, it takes over a half second for it to reach the second operating point. At first this seems wrong, but it is not. The inertia of the machine is very large and therefore resists changes in rotation. During this time the torque being provided is limited by the upper bound of the safe operating region.

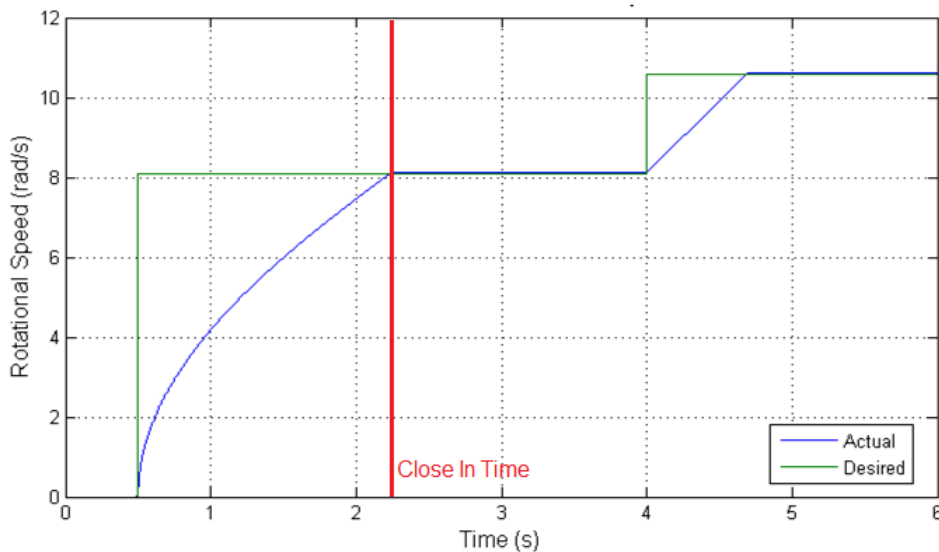


Figure 4-6. Mechanical Rotational Speed Comparison Plot

The slow transient present in this figure will not cause a problem in actual operation. There are no step functions in nature, especially in water. As discussed earlier, the high density of water makes it resist changes in velocity. This means that the change in desired rotational speed should change slow enough that the controller will be able to follow it.

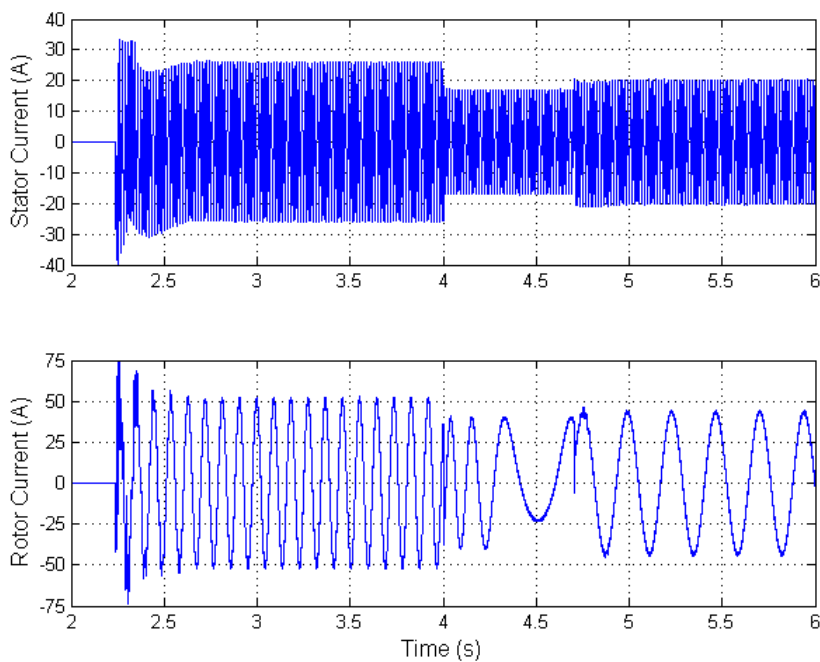


Figure 4-7. DFIM Stator and Rotor A Phase Current Plots

Figure 4-7 shows the A phase current waveforms for the DFIM during this simulation. The magnitudes of these waveforms are very close to those predicted by steady state analysis. In the first operating zone, the stator and rotor currents are approximately 25.5 A and 52 A respectively. They should be approximately 25.5 A and 52.6 A. During the second steady state zone, the actual currents were about 20 A and 43.5 A compared to the predicted 19.1 A and 44.6 A for stator and rotor respectively. These currents are very close, but not exact. Some explanation for these differences may come from examining the stator real and reactive power plots found in Figure 4-8.

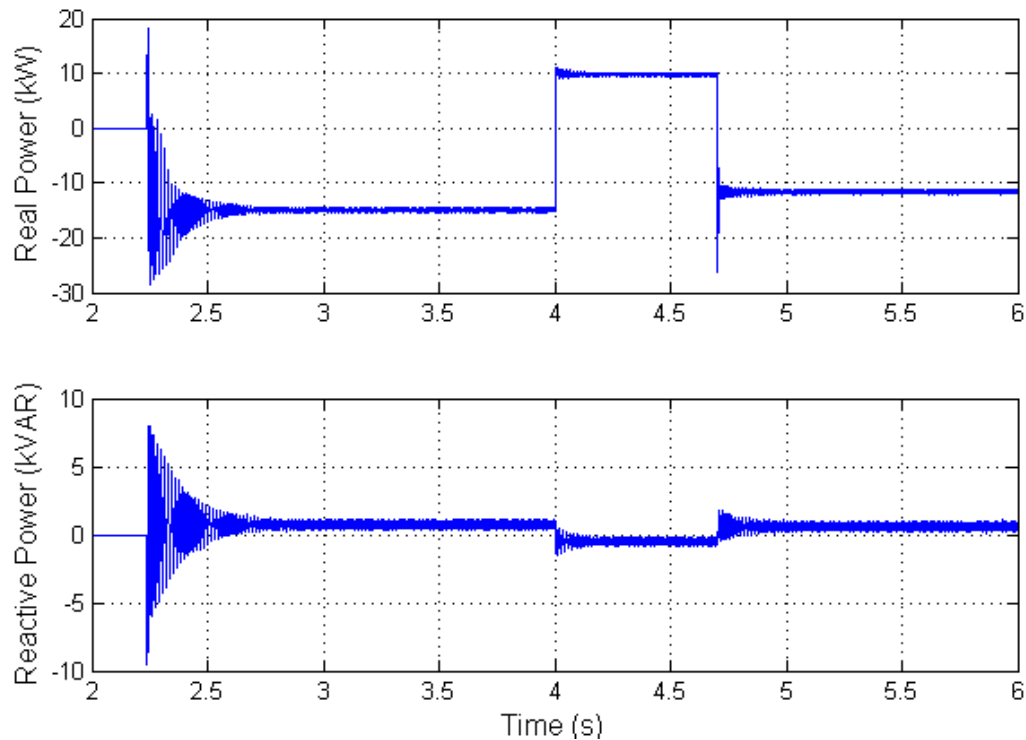


Figure 4-8. DFIM Real and Reactive Power Plots

The real power in these plots almost exactly matches the predicted values. The problem here is that the reactive power Q is non zero, even though it was commanded to be zero. This reactive power is most likely responsible for the minor current variations shown earlier. The problem with reactive power can be fixed by adding an outer loop reactive feedback controller to verify that the reactive power meets its desired value.

4.6 SUMMARY

This chapter provides an overview of the methods used to model the various components of the hydrokinetic generation system in Simulink[®]. Both the mechanical and electrical system designs were covered in detail. This chapter also provided details on the control systems used to control the application. Although some of the controllers may not be the ideal solution, the system behaves in the desired fashion. This is proven by the simulation results presented in the last section. All the values shown are within tolerance with the values predicted using steady state analysis and clearly shows that the control system can track along with changes in input velocity. The response of this system could be improved by adding a feedback controller on the reactive power input so that it will be forced to its desired value.

In the application simulated here, the only input to the system was the velocity of the water flow. Using this velocity, the controller then calculated the optimum rotational speed to produce the most power generation possible. Then, the machine responded to operate at this speed, generating currents within tolerance of the values predicted by steady state analysis. This shows that both the machine and control system meet the desired performance they were designed for.

4.7 REFERENCES

- [1] A. Yazdani and R. Iravani, *Voltage-Sourced Converters in Power Systems*. Hoboken, NJ: Wiley-IEEE Press, 2010.
- [2] G. Abad et al., *Doubly Fed Induction Machine: Modeling and Control for Wind Energy Generation Applications*. Hoboken, NJ: Wiley-IEEE Press, 2011.
- [3] C.R. Nave, "Thick Hoops and Hollow Cylinders," *HyperPhysics*, 2012. [Online]. Available: <http://hyperphysics.phy-astr.gsu.edu/hbase/ihoop.html#ihoop2>. [Accessed: June 28, 2014].
- [4] B. Wu et al., *Power Conversion and Control of Wind Energy Systems*. Hoboken, NJ: Wiley-IEEE Press, 2011.

CHAPTER 5: CONCLUSIONS

5.1 SUMMARY

America is demanding new sources of clean energy production. The wind industry has been growing rapidly by providing what appears, on the surface, to be a free endless source of energy. In pursuit of improving this technology there have been many advancements made in the design of both mechanical and electrical systems. Unfortunately, when onshore wind turbines are honestly examined, they are, in truth, an ineffective technology with enormous potential to damage the environment, both for people and wild life. Fortunately, many of the advancements made for wind can be applied to an older concept of in-stream hydroelectric generation, also referred to as hydrokinetic generation. One such advancement is the application of a gearless doubly fed induction machine topology. The goal of this thesis was ultimately to show the viability of this concept so that future research can be conducted to make this a reality.

In order to apply the gearless DFIM for this application, it was necessary to first examine the options available when designing the mechanical system and how much energy is available for generation. There are several choices a turbine designer must consider when designing their turbine including orientation, number of blades, mooring, and the use of augmentation. Each of these options will directly affect the efficiency and cost of the application. Once a turbine has been specified, it is necessary to determine placement and location. As discussed earlier, a good way to do this is by examining multiple locations looking for the overall optimum design, and then picking the location that best fits desired criteria.

With a mechanical system specified, the next step was to actually design the DFIM. This thesis presented background on the concepts and formulas necessary for the design of any AC machine including winding theory as well as full calculation of resistance and inductances including the leakage terms. With this information, a method for designing a DFIM to meet a specific mechanical power and speed rating was presented. This method used two main equations that could be applied, along with some rules of thumb, to the stator and rotor of the machine in order to determine a viable design. The full parameters of the DFIM were presented and the calculations can be found in Appendix A.

A model of the system was created and simulated in Simulink[®]. The components of the model discussed in this document include the water turbine, mechanical coupling, lossless non-idealized two level voltage source converter, and DFIM itself. In addition, several control elements were included in the simulation. These include an overarching controller which uses the water speed to determine desired mechanical rotational speed using a unique algorithm to maximize power generated, a rotational speed controller, a current reference calculator, as well as current control loops. The results presented demonstrate proper operation of the overall system that aligns with steady state calculations.

The hydrokinetic turbine may be an old idea, but it is a good one that can be greatly improved upon with modern advances in technology. It is time that governments and corporations take the money they are throwing into the wind, and instead invest in a technology with actual potential to improve the future of the planet and its people.

5.2 FUTURE WORK

There is a lot of work necessary in order for the application presented here to become a reality and even more that can be done to improve upon it. There are several things that need to be done before this machine can be built full scale. Before any construction can begin, a team of mechanical engineers needs to determine an appropriate method of mounting the machine inside the duct; this will include determining mounting, bearings, and a method for water proofing. Since the turbine is underwater, it must be water proofed and, therefore, cannot use conventional forced air cooling. In addition, the short length of the machine makes ducts unfeasible. Before moving forward, a full thermal analysis must be done on the system to verify that the temperature of the machine will not exceed an acceptable level. Once this is done, a small scale prototype should be constructed so that it can be tested to verify both the electrical parameter design as well as the overall operation.

Using the basic USGS data may be acceptable for a proof of concept, but not for a commercial application. This data may be valuable at determining an actual location, but should not be used in actual design. This data is only taken at a specific point in the river or stream and is only provided as discharge data. To ensure accuracy, actual velocity data at multiple depths should be taken nearly continuously over the course of at least a year. In

addition, the full topology of the stream should be considered such as the shape of the stream bed and how much it increases or decreases in width over that same time period. This data will provide for a much more accurate picture of what can actually be generated.

The application presented here is rather crude and can be fine tuned in many ways. First off, the turbine chosen here was designed over 30 years ago for a traditional induction machine application. There have been many advancements in the overall theory and tools for turbine design, such as computational fluid dynamics, that could lead to far better turbine design. In addition, knowing that the DFIM is going to be used may allow for power coefficient vs. tip speed ratio curve to be designed in such a way as to fully use the capabilities of the machine.

Another way to improve the design would be to determine a better method for determining the potential of the streams. The current method could be improved by determining optimization constants actually based on relative cost or financial benefit. In addition, this algorithm might be able to be improved to verify that the DFIM is living up to its full potential.

The design of the DFIM also leaves room for improvement. Instead of using only series windings, parallel could be used which allow for potentially easier construction and lower losses. Also, in this design, the slots were assumed to have an even width from top to bottom, but this does not have to be the case, especially if smaller wires are used in parallel. The top of the slots can be smaller than the base which could help decrease inductive losses. The back iron width was chosen semi arbitrarily, but an optimum value could be calculated to avoid saturation. This could reduce the thickness of the iron which, in turn, would reduce weight, inertia, and cost.

Another idea for improvement, would be to move the scope beyond just Idaho. There are other states with far more water resources such as Washington, Oregon, and California. The Columbia River is a huge resource that may still hold a lot of potential. These turbines will only take up a percentage of the water way leaving the rest for wildlife and transportation lanes, therefore they should have minimal environmental impact.

Areas of research regarding hydrokinetic turbines is almost limitless and would be a far better use of resources than wind turbine research. In the end, it could lead to a more reliable and commercially viable technology than wind will ever be.

APPENDIX A: MATHCAD DFIM DESIGN SHEET

Grid-Connected In-Stream Hydroelectric Generation Based on the Doubly Fed Induction Machine	DFIM Design Sheet	Timothy Lenberg Graduate Student University of Idaho
---	-------------------	--

$E_s := 480V$		Desired Line to Line Stator Voltage
$P_s := 10kW$		Desired Rated Stator Power
$f_s := 60Hz$		Grid Frequency
$P_r := .3 \cdot P_s$	$P_r = 3 \cdot kW$	Desired Rated Rotor Power
$f_r := .3 \cdot f_s$	$f_r = 18 \cdot Hz$	Desired Rotor Frequency
$D_o := 2.78m$		Outer Diameter of Turbine
$C_o := \frac{D_o}{10ft}$	$C_o = 0.912$	Scaling Factor
$D := C_o \cdot \frac{63}{31}m$	$D = 1.854m$	Diameter of Air Gap
$q := 3$		Phase Belts Per Pole
$L_1 := \frac{15}{62}m \cdot C_o$	$L_1 = 0.221m$	Length of Machine Iron
$t_{fe} := C_o \cdot \frac{5}{62}m$	$t_{fe} = 73.554 \cdot mm$	Max Thickness of Iron
$P_1 := 38$		Desired Pole Pairs
$I_s := \frac{P_s}{\sqrt{3} \cdot E_s}$	$I_s = 12.028 A$	Stator Current Per Phase
$g_1 := \frac{.01 \cdot \pi \cdot D}{2 \cdot P_1}$	$g_1 = 0.766 \cdot mm$	Actual Air Gap
$n_s := \text{floor} \left[\frac{\left[\frac{\pi \cdot (D + g_1)}{.5in} \right]}{2 \cdot q \cdot P_1} \right]$	$n_s = 2$	Stator Slots Per Phase Belt
$n_r := \text{floor} \left[\frac{\left[\frac{\pi \cdot (D - g_1)}{.5in} \right]}{2 \cdot q \cdot P_1} \right]$	$n_r = 2$	Rotor Slots Per Phase Belt
$p_s := \frac{\text{floor} \left(n_s \cdot q \cdot \frac{5}{6} \right)}{n_s \cdot q}$	$p_s = \frac{5}{6}$	Stator Winding Pitch
$p_r := \frac{\text{floor} \left(n_r \cdot q \cdot \frac{5}{6} \right)}{n_r \cdot q}$	$p_r = \frac{5}{6}$	Rotor Winding Pitch

$$K_{ps}(h) := \sin\left(\frac{h \cdot P_s \cdot \pi}{2}\right) \cdot \sin\left(\frac{h \cdot \pi}{2}\right)$$

Stator Pitch Factor

$$K_{pr}(h) := \sin\left(\frac{h \cdot P_r \cdot \pi}{2}\right) \cdot \sin\left(\frac{h \cdot \pi}{2}\right)$$

Rotor Pitch Factor

$$K_{ds}(h) := \frac{\sin\left(\frac{h \cdot \pi}{2 \cdot q}\right)}{n_s \cdot \sin\left(\frac{h \cdot \pi}{2 \cdot n_s \cdot q}\right)}$$

Stator Winding Distribution Factor

$$K_{dr}(h) := \frac{\sin\left(\frac{h \cdot \pi}{2 \cdot q}\right)}{n_r \cdot \sin\left(\frac{h \cdot \pi}{2 \cdot n_r \cdot q}\right)}$$

Rotor Winding Distribution Factor

$$\text{Slots}_s := q \cdot P_1 \cdot 2 \cdot n_s$$

$$\text{Slots}_s = 456$$

Total Number of Stator Slots

$$\text{Slots}_r := q \cdot P_1 \cdot 2 \cdot n_r$$

$$\text{Slots}_r = 456$$

Total Number of Rotor Slots

$$\tau_s := \frac{\pi \cdot (D + g_1)}{\text{Slots}_s}$$

$$\tau_s = 12.775 \cdot \text{mm}$$

Width of 1 stator slot and tooth

$$\tau_r := \frac{\pi \cdot (D - g_1)}{\text{Slots}_r}$$

$$\tau_r = 12.765 \cdot \text{mm}$$

Width of 1 rotor slot and tooth

$$\tau_{ps} := n_s \cdot q \cdot \tau_s$$

$$\tau_{ps} = 76.652 \cdot \text{mm}$$

Length of one pole pitch stator

$$\tau_{pr} := n_r \cdot q \cdot \tau_s$$

$$\tau_{pr} = 76.652 \cdot \text{mm}$$

Length of one pole pitch rotor



$$\text{width}_1 := .04 \text{mm}$$

$$\text{num}_s(\text{AWG}_s) := \text{floor} \left[\frac{2 \cdot \left(\frac{D}{2} + \frac{g_1}{2} \right)^2 \cdot \left(1 - \cos \left(\frac{.54 \cdot \tau_s}{\frac{D}{2} + \frac{g_1}{2}} \right) \right)}{\text{wired}_{\text{AWG}_s} + \text{width}_1} \right]$$

$$\text{num}_r := 1$$

Grid-Connected In-Stream Hydroelectric Generation Based on the Doubly Fed Induction Machine	DFIM Design Sheet	Timothy Lenberg Graduate Student University of Idaho
---	-------------------	--

$$b_{os}(AWG_s) := \left(\frac{D}{2} + \frac{g_1}{2}\right) \cdot \text{acos} \left[1 - \frac{\left[\text{num}_s(AWG_s) \cdot (\text{wired}_{AWG_s} + \text{width}_i) \right]^2}{2 \cdot \left(\frac{D}{2} + \frac{g_1}{2}\right)^2} \right] + \text{width}_i$$

$$b_{or}(AWG_r) := \left(\frac{D}{2} - \frac{g_1}{2}\right) \cdot \text{acos} \left[1 - \frac{\left[\text{num}_r(\text{wired}_{AWG_r} + \text{width}_i) \right]^2}{2 \cdot \left(\frac{D}{2} - \frac{g_1}{2}\right)^2} \right] + \text{width}_i$$

$$t_{os}(AWG_s) := \tau_s - b_{os}(AWG_s)$$

$$t_{or}(AWG_r) := \tau_r - b_{or}(AWG_r)$$

$$k_{cs}(AWG_s) := \frac{\tau_s}{\tau_s - \frac{2 \cdot b_{os}(AWG_s)}{\pi} \left[\text{atan} \left(\frac{b_{os}(AWG_s)}{2 \cdot g_1} \right) - \frac{g_1}{b_{os}(AWG_s)} \cdot \ln \left[1 + \left(\frac{b_{os}(AWG_s)}{2 \cdot g_1} \right)^2 \right] \right]}$$

$$k_{cr}(AWG_r) := \frac{\tau_r}{\tau_r - \frac{2 \cdot b_{or}(AWG_r)}{\pi} \left[\text{atan} \left(\frac{b_{or}(AWG_r)}{2 \cdot g_1} \right) - \frac{g_1}{b_{or}(AWG_r)} \cdot \ln \left[1 + \left(\frac{b_{or}(AWG_r)}{2 \cdot g_1} \right)^2 \right] \right]}$$

$$k_c(AWG_s, AWG_r) := k_{cs}(AWG_s) \cdot k_{cr}(AWG_r)$$

$$g_e(AWG_s, AWG_r) := k_c(AWG_s, AWG_r) \cdot g_1$$

$$\chi_s(AWG_s) := \text{acos} \left[1 - \frac{b_{os}(AWG_s)^2}{2 \cdot \left(\frac{D}{2} + \frac{g_1}{2}\right)^2} \right] \cdot \frac{P_1}{2}$$

$$\chi_r(AWG_r) := \text{acos} \left[1 - \frac{b_{or}(AWG_r)^2}{2 \cdot \left(\frac{D}{2} - \frac{g_1}{2}\right)^2} \right] \cdot \frac{P_1}{2}$$

Optimization Attempt_v2.0 480V.xmcd	Page 3 of 17	June 30, 2014
--	--------------	---------------

$$K_{\chi_s}(h, AWG_s) := \text{sinc}\left(\frac{h \cdot \chi_s(AWG_s)}{2}\right)$$

$$K_{\chi_r}(h, AWG_r) := \text{sinc}\left(\frac{h \cdot \chi_r(AWG_r)}{2}\right)$$

$$\sigma_s := \frac{P_1 \cdot 2 \cdot \pi}{\text{Slots}_s}$$

$$\sigma_r := \frac{P_1 \cdot 2 \cdot \pi}{\text{Slots}_r}$$

$$\text{Skew}_s := 2$$

$$\text{Skew}_r := 0$$

$$\alpha_s := \text{Skew}_s \cdot \sigma_s$$

$$\alpha_r := \text{Skew}_r \cdot \sigma_r$$

$$K_{ss}(h) := \text{sinc}\left(\frac{h \cdot \alpha_s}{2}\right)$$

$$K_{sr}(h) := \text{sinc}\left(\frac{h \cdot \alpha_r}{2}\right)$$

$$K_s(h, AWG_s) := \begin{cases} 0 & \text{if } \text{floor}\left(\frac{h}{3}\right) - \frac{h}{3} = 0 \\ (K_{ps}(h) \cdot K_{ds}(h) \cdot K_{\chi_s}(h, AWG_s) \cdot K_{ss}(h)) & \text{otherwise} \end{cases}$$

$$K_r(h, AWG_r) := \begin{cases} 0 & \text{if } \text{floor}\left(\frac{h}{3}\right) - \frac{h}{3} = 0 \\ (K_{pr}(h) \cdot K_{dr}(h) \cdot K_{\chi_r}(h, AWG_r) \cdot K_{sr}(h)) & \text{otherwise} \end{cases}$$

$$\rho_{\text{copper}70} := 1.72 \cdot 10^{-8} \cdot \Omega \cdot \text{m} \cdot [1 + .00426 \cdot (70 - 20)] \quad \rho_{\text{copper}70} = 2.086 \times 10^{-8} \cdot \Omega \cdot \text{m}$$

$$R_s(N_s, AWG_s) := \frac{\left[\sqrt{L_1^2 + (\text{Skew}_s \cdot \tau_s)^2} + p_s \cdot \tau_{ps} + \text{wired}_{AWG_s} \right] \cdot 2 \cdot N_s \cdot \rho_{\text{copper}70}}{\pi \cdot \left(\frac{\text{wired}_{AWG_s}}{2} \right)^2}$$

$$R'_I(N_I, AWG_I) := \frac{\left[\sqrt{L_1^2 + (\text{Skew}_I \cdot \tau_I)^2} + p_I \cdot \tau_{pr} + \text{wired}_{AWG_I} \right] \cdot 2 \cdot N_I \cdot \rho_{\text{copper70}}}{\pi \cdot \left(\frac{\text{wired}_{AWG_I}}{2} \right)^2}$$

$$T_S(N_S) := \frac{3 \cdot N_S}{\text{Slots}_S}$$

$$T_I(N_I) := \frac{3 \cdot N_I}{\text{Slots}_I}$$

$$\text{Depth}_{\text{sslot}}(N_S, AWG_S) := \frac{2 \cdot T_S(N_S) \cdot (\text{wired}_{AWG_S} + \text{width}_I)}{\text{num}_S(AWG_S)} + \text{width}_I$$

$$\text{Depth}_{\text{rslot}}(N_I, AWG_I) := \frac{2 \cdot T_I(N_I) \cdot (\text{wired}_{AWG_I} + \text{width}_I)}{\text{num}_I} + \text{width}_I$$

$$N_{\text{se}}(N_S, AWG_S) := \frac{4}{\pi} \cdot K_S(1, AWG_S) \cdot N_S$$

$$N_{\text{re}}(N_I, AWG_I) := \frac{4}{\pi} \cdot K_I(1, AWG_I) \cdot N_I$$

$$r := \frac{D}{2}$$

$$L_{\text{ms}}(N_S, AWG_S, AWG_I) := \frac{3}{2} \cdot \left(\frac{N_{\text{se}}(N_S, AWG_S)}{2 \cdot p_1} \right)^2 \cdot \mu_0 \cdot \pi \cdot \frac{r \cdot L_1}{g_e(AWG_S, AWG_I)}$$

$$L_{\text{mr}}(N_I, AWG_S, AWG_I) := \frac{3}{2} \cdot \left(\frac{N_{\text{re}}(N_I, AWG_I)}{2 \cdot p_1} \right)^2 \cdot \mu_0 \cdot \pi \cdot \frac{r \cdot L_1}{g_e(AWG_S, AWG_I)}$$

$$b_{\text{ss}}(AWG_S) := b_{\text{os}}(AWG_S)$$

$$b_{\text{sr}}(AWG_I) := b_{\text{or}}(AWG_I)$$

$$d_{0S} := 0$$

$$d_{0I} := 0$$

$$d_{1S} := 0$$

$$d_{1r} := 0$$

$$d_{2s} := \text{width}_i$$

$$d_{2r} := \text{width}_i$$

$$d_{4s} := \text{width}_i$$

$$d_{4r} := \text{width}_i$$

$$d_{6s} := \text{width}_i$$

$$d_{6r} := \text{width}_i$$

$$d_{3s}(N_s, \text{AWG}_s) := \frac{\text{Depth}_{\text{sslots}}(N_s, \text{AWG}_s) - d_{0s} - d_{1s} - d_{4s} - d_{6s}}{2}$$

$$d_{3r}(N_r, \text{AWG}_r) := \frac{\text{Depth}_{\text{rslots}}(N_r, \text{AWG}_r) - d_{0r} - d_{1r} - d_{4r} - d_{6r}}{2}$$

$$d_{5s}(N_s, \text{AWG}_s) := d_{3s}(N_s, \text{AWG}_s)$$

$$d_{5r}(N_r, \text{AWG}_r) := d_{3r}(N_r, \text{AWG}_r)$$

$$\rho_{Ts}(N_s, \text{AWG}_s) := \mu_0 \cdot \left(\frac{d_{3s}(N_s, \text{AWG}_s)}{3 \cdot b_{ss}(\text{AWG}_s)} + \frac{d_{2s}}{b_{ss}(\text{AWG}_s)} \dots \right. \\ \left. + \frac{d_{1s}}{b_{ss}(\text{AWG}_s) - b_{os}(\text{AWG}_s) + 10^{-16} \text{mm}} \cdot \ln \left(\frac{b_{ss}(\text{AWG}_s)}{b_{os}(\text{AWG}_s)} \right) + \frac{d_{0s}}{b_{os}(\text{AWG}_s)} \right)$$

$$\rho_{Tr}(N_r, \text{AWG}_r) := \mu_0 \cdot \left(\frac{d_{3r}(N_r, \text{AWG}_r)}{3 \cdot b_{sr}(\text{AWG}_r)} + \frac{d_{2r}}{b_{sr}(\text{AWG}_r)} \dots \right. \\ \left. + \frac{d_{1r}}{b_{sr}(\text{AWG}_r) - b_{or}(\text{AWG}_r) + 10^{-16} \text{mm}} \cdot \ln \left(\frac{b_{sr}(\text{AWG}_r)}{b_{or}(\text{AWG}_r)} \right) + \frac{d_{0r}}{b_{or}(\text{AWG}_r)} \right)$$

$$\rho_{Bs}(N_s, \text{AWG}_s) := \mu_0 \cdot \left(\frac{d_{5s}(N_s, \text{AWG}_s)}{3 \cdot b_{ss}(\text{AWG}_s)} + \frac{d_{2s} + d_{3s}(N_s, \text{AWG}_s) + d_{4s}}{b_{ss}(\text{AWG}_s)} \dots \right. \\ \left. + \frac{d_{1s}}{b_{ss}(\text{AWG}_s) - b_{os}(\text{AWG}_s) + 10^{-16} \text{mm}} \cdot \ln \left(\frac{b_{ss}(\text{AWG}_s)}{b_{os}(\text{AWG}_s)} \right) + \frac{d_{0s}}{b_{os}(\text{AWG}_s)} \right)$$

Grid-Connected In-Stream Hydroelectric Generation Based on the Doubly Fed Induction Machine	DFIM Design Sheet	Timothy Lenberg Graduate Student University of Idaho
---	-------------------	--

$$\rho_{Br}(N_r, AWG_r) := \mu_0 \cdot \left(\frac{d_{5r}(N_r, AWG_r)}{3 \cdot b_{sr}(AWG_r)} + \frac{d_{2r} + d_{3r}(N_r, AWG_r) + d_{4r}}{b_{sr}(AWG_r)} \dots \right. \\ \left. + \frac{d_{1r}}{b_{sr}(AWG_r) - b_{or}(AWG_r) + 10^{-16} \text{ mm}} \cdot \ln \left(\frac{b_{sr}(AWG_r)}{b_{or}(AWG_r)} \right) + \frac{d_{0r}}{b_{or}(AWG_r)} \right)$$

$$\rho_{Tbs}(N_s, AWG_s) := \mu_0 \cdot \left(\frac{d_{0s}}{b_{os}(AWG_s)} + \frac{d_{1s}}{b_{ss}(AWG_s) - b_{os}(AWG_s) + 10^{-16} \text{ mm}} \cdot \ln \left(\frac{b_{ss}(AWG_s)}{b_{os}(AWG_s)} \right) \dots \right. \\ \left. + \frac{d_{2s}}{b_{ss}(AWG_s)} + \frac{d_{3s}(N_s, AWG_s)}{2 \cdot b_{ss}(AWG_s)} \right)$$

$$\rho_{Tbr}(N_r, AWG_r) := \mu_0 \cdot \left(\frac{d_{0r}}{b_{or}(AWG_r)} + \frac{d_{1r}}{b_{sr}(AWG_r) - b_{or}(AWG_r) + 10^{-16} \text{ mm}} \cdot \ln \left(\frac{b_{sr}(AWG_r)}{b_{or}(AWG_r)} \right) \dots \right. \\ \left. + \frac{d_{2r}}{b_{sr}(AWG_r)} + \frac{d_{3r}(N_r, AWG_r)}{2 \cdot b_{sr}(AWG_r)} \right)$$

$$L_{IBs}(N_s, AWG_s) := 3 \cdot N_s^2 \cdot \frac{L_1}{\text{Slots}_s} \cdot \rho_{Bs}(N_s, AWG_s)$$

$$L_{IBr}(N_r, AWG_r) := 3 \cdot N_r^2 \cdot \frac{L_1}{\text{Slots}_r} \cdot \rho_{Br}(N_r, AWG_r)$$

$$L_{ITs}(N_s, AWG_s) := 3 \cdot N_s^2 \cdot \frac{L_1}{\text{Slots}_s} \cdot \rho_{Ts}(N_s, AWG_s)$$

$$L_{ITr}(N_r, AWG_r) := 3 \cdot N_r^2 \cdot \frac{L_1}{\text{Slots}_r} \cdot \rho_{Tr}(N_r, AWG_r)$$

$$L_{IMs}(N_s, AWG_s) := 3 \cdot N_s^2 \cdot \frac{L_1}{\text{Slots}_s} \cdot \rho_{Tbs}(N_s, AWG_s)$$

$$L_{IMr}(N_r, AWG_r) := 3 \cdot N_r^2 \cdot \frac{L_1}{\text{Slots}_r} \cdot \rho_{Tbr}(N_r, AWG_r)$$

$$k_{sl}(p) := \begin{cases} (3p - 1) & \text{if } \frac{2}{3} < p \leq 1 \\ [3 \cdot (2 \cdot p - 1)] & \text{if } \frac{1}{3} < p \leq \frac{2}{3} \\ (3 \cdot p - 2) & \text{if } 0 < p \leq \frac{1}{3} \end{cases}$$

$$L_{slots}(N_s, AWG_s) := L_{ITs}(N_s, AWG_s) + L_{IBs}(N_s, AWG_s) + k_{sl}(p_s) \cdot L_{IMs}(N_s, AWG_s)$$

$$L_{slotr}(N_r, AWG_r) := L_{ITr}(N_r, AWG_r) + L_{IBr}(N_r, AWG_r) + k_{sl}(p_r) \cdot L_{IMr}(N_r, AWG_r)$$

$$\epsilon_s(AWG_s) := \frac{\text{wired}_{AWG_s}}{2}$$

$$\epsilon_r(AWG_r) := \frac{\text{wired}_{AWG_r}}{2}$$

$$a_s(AWG_s) := \epsilon_s(AWG_s) \cdot 2$$

$$a_r(AWG_r) := \epsilon_r(AWG_r) \cdot 2$$

$$b_s := \tau_{ps} \cdot p_s$$

$$b_r := \tau_{pr} \cdot p_r$$

Perfect Conductor Model

$$L_{ew1_pcs}(AWG_s) := \frac{\mu_0}{\pi} \left[\begin{aligned} & -2 \cdot a_s(AWG_s) \cdot \ln \left[\frac{2 \cdot a_s(AWG_s)}{b_s} + \sqrt{\left(\frac{2 \cdot a_s(AWG_s)}{b_s} \right)^2 + 1} \right] \dots \\ & + b_s \cdot \ln \left[\frac{b_s}{2 a_s(AWG_s)} + \sqrt{\left(\frac{b_s}{2 a_s(AWG_s)} \right)^2 + 1} \right] \dots \\ & + 2 a_s(AWG_s) \cdot \ln \left(\frac{4 a_s(AWG_s)}{\epsilon_s(AWG_s)} \right) + b_s \cdot \ln \left(\frac{2 \cdot b_s}{\epsilon_s(AWG_s)} \right) \dots \\ & + 2 \cdot \sqrt{4 a_s(AWG_s)^2 + b_s^2} - 2 b_s - 4 a_s(AWG_s) \end{aligned} \right]$$

$$L_{ew1_pdr}(AWG_r) := \frac{\mu_0}{\pi} \left[\begin{aligned} & -2 \cdot a_r(AWG_r) \cdot \ln \left[\frac{2 \cdot a_r(AWG_r)}{b_r} + \sqrt{\left(\frac{2 \cdot a_r(AWG_r)}{b_r} \right)^2 + 1} \right] \dots \\ & + b_r \cdot \ln \left[\frac{b_r}{2 a_r(AWG_r)} + \sqrt{\left(\frac{b_r}{2 a_r(AWG_r)} \right)^2 + 1} \right] \dots \\ & + 2 a_r(AWG_r) \cdot \ln \left(\frac{4 a_r(AWG_r)}{\epsilon_r(AWG_r)} \right) + b_r \cdot \ln \left(\frac{2 \cdot b_r}{\epsilon_r(AWG_r)} \right) \dots \\ & + 2 \cdot \sqrt{4 a_r(AWG_r)^2 + b_r^2} - 2 b_r - 4 a_r(AWG_r) \end{aligned} \right]$$

Air Model

$$L_{ew1_as}(AWG_s) := \frac{\mu_0}{2 \cdot \pi} \left[\begin{aligned} & -2 \cdot \sqrt{a_s(AWG_s)^2 + b_s^2} + 3 \cdot \sqrt{4 a_s(AWG_s)^2 + b_s^2} - 4 a_s(AWG_s) - b_s \dots \\ & + 2 a_s(AWG_s) \cdot \ln \left[\frac{2 \left(a_s(AWG_s) + \sqrt{a_s(AWG_s)^2 + b_s^2} \right)}{b_s} \right] \dots \\ & + -4 a_s(AWG_s) \cdot \ln \left(\frac{2 a_s(AWG_s) + \sqrt{4 a_s(AWG_s)^2 + b_s^2}}{2 \cdot b_e} \right) \dots \\ & + 2 a_s(AWG_s) \cdot \ln \left(\frac{\epsilon_s(AWG_s)}{b_s} \right) + 2 a_s(AWG_s) \cdot \ln \left(\frac{4 a_s(AWG_s)}{\epsilon_s(AWG_s)} \right) \dots \\ & + b_s \cdot \ln \left[\frac{b_s}{2 a_s(AWG_s)} + \sqrt{\left(\frac{b_s}{2 a_s(AWG_s)} \right)^2 + 1} \right] \dots \\ & + b_s \cdot \ln \left[\frac{b_s}{\epsilon_s(AWG_s)} + \sqrt{\left(\frac{b_s}{\epsilon_s(AWG_s)} \right)^2 + 1} \right] \end{aligned} \right]$$

$$L_{ew1_ar}(AWG_r) := \frac{\mu_0}{2 \cdot \pi} \cdot \left[\begin{aligned} & -2 \cdot \sqrt{a_r(AWG_r)^2 + b_r^2} + 3 \cdot \sqrt{4 a_r(AWG_r)^2 + b_r^2} - 4 a_r(AWG_r) - b_r \dots \\ & + 2 \cdot a_r(AWG_r) \cdot \ln \left[\frac{2(a_r(AWG_r) + \sqrt{a_r(AWG_r)^2 + b_r^2})}{b_r} \right] \dots \\ & + -4 a_r(AWG_r) \cdot \ln \left(\frac{2 a_r(AWG_r) + \sqrt{4 a_r(AWG_r)^2 + b_r^2}}{2 \cdot b_r} \right) \dots \\ & + 2 a_r(AWG_r) \cdot \ln \left(\frac{\epsilon_r(AWG_r)}{b_r} \right) + 2 a_r(AWG_r) \cdot \ln \left(\frac{4 a_r(AWG_r)}{\epsilon_r(AWG_r)} \right) \dots \\ & + -b_r \cdot \ln \left[\frac{b_r}{2 a_r(AWG_r)} + \sqrt{\left(\frac{b_r}{2 a_r(AWG_r)} \right)^2 + 1} \right] \dots \\ & + b_r \cdot \ln \left[\frac{b_r}{\epsilon_r(AWG_r)} + \sqrt{\left(\frac{b_r}{\epsilon_r(AWG_r)} \right)^2 + 1} \right] \end{aligned} \right]$$

Average

$$L_{ew1_s}(AWG_s) := \frac{L_{ew1_as}(AWG_s) + L_{ew1_pcs}(AWG_s)}{2}$$

$$L_{ew1_r}(AWG_r) := \frac{L_{ew1_ar}(AWG_r) + L_{ew1_pcr}(AWG_r)}{2}$$

$$L_{ews}(N_s, AWG_s) := \frac{2}{2 \cdot P_1} \cdot K_{ds}(1)^2 \cdot K_{ps}(1)^2 \cdot N_s^2 \cdot L_{ew1_s}(AWG_s)$$

$$L_{ewr}(N_r, AWG_r) := \frac{2}{2 \cdot P_1} \cdot K_{dr}(1)^2 \cdot K_{pr}(1)^2 \cdot N_r^2 \cdot L_{ew1_r}(AWG_r)$$

$$L_{lks}(N_s, AWG_s, AWG_r) := L_{ms}(N_s, AWG_s, AWG_r) \cdot \left[\frac{1}{K_s(1, AWG_s)^2} \cdot \sum_{h=2}^{1000} \left(\frac{K_s(h, AWG_s)}{h} \right)^2 \right]$$

$$L_{lkr}(N_r, AWG_s, AWG_r) := L_{mr}(N_r, AWG_s, AWG_r) \cdot \left[\frac{1}{K_r(1, AWG_r)^2} \cdot \sum_{h=2}^{1000} \left(\frac{K_r(h, AWG_r)}{h} \right)^2 \right]$$

$$\rho_{zss}(AWG_s, AWG_r) := \frac{\mu_0 \cdot t_{os}(AWG_s) \cdot t_{or}(AWG_r) \cdot (t_{or}(AWG_r)^2 + t_{os}(AWG_s)^2)}{6 \cdot g_e(AWG_s, AWG_r) \cdot \tau_s^3}$$

$$\rho_{ZZI}(AWG_s, AWG_r) := \frac{\mu_0 \cdot t_{os}(AWG_s) \cdot t_{or}(AWG_r) \cdot (t_{or}(AWG_r)^2 + t_{os}(AWG_s)^2)}{6 \cdot g_{el}(AWG_s, AWG_r) \cdot \tau_r^3}$$

$$L_{IZZ}(N, S, p, \rho_{ZZ}) := \begin{cases} \left[\frac{3 \cdot N^2}{S} \cdot L_1 \cdot \frac{(21p - 5)}{4} \cdot \rho_{ZZ} \right] & \text{if } \frac{2}{3} < p \leq 1 \\ \left(\frac{27}{4} \cdot N^2 \cdot \frac{L_1}{S} \cdot \rho_{ZZ} \right) & \text{if } \frac{1}{3} < p \leq \frac{2}{3} \\ \left(3 \cdot N^2 \cdot \frac{L_1}{S} \cdot \frac{27p}{4} \cdot \rho_{ZZ} \right) & \text{if } 0 < p \leq \frac{1}{3} \end{cases}$$

$$L_{Izzs}(N_s, AWG_s, AWG_r) := L_{IZZ}(N_s, Slots_s, p_s, \rho_{ZZs}(AWG_s, AWG_r))$$

$$L'_{Izzr}(N_r, AWG_s, AWG_r) := L_{IZZ}(N_r, Slots_r, p_r, \rho_{ZZr}(AWG_s, AWG_r))$$

$$L_{Isks}(N_s, AWG_s, AWG_r) := L_{ms}(N_s, AWG_s, AWG_r) \cdot \frac{(1 - K_{ss}(1)^2)}{K_{ss}(1)}$$

$$L'_{Iskr}(N_r, AWG_s, AWG_r) := L'_{mr}(N_r, AWG_s, AWG_r) \cdot \frac{(1 - K_{sr}(1)^2)}{K_{sr}(1)}$$

$$L_s(N_s, AWG_s, AWG_r) := L_{slots}(N_s, AWG_s) + L_{ews}(N_s, AWG_s) + L_{lks}(N_s, AWG_s, AWG_r) \dots \\ + L_{Izzs}(N_s, AWG_s, AWG_r) + L_{Isks}(N_s, AWG_s, AWG_r)$$

$$L'_r(N_r, AWG_s, AWG_r) := L'_{slotr}(N_r, AWG_r) + L'_{ewr}(N_r, AWG_r) + L'_{lkr}(N_r, AWG_s, AWG_r) \dots \\ + L'_{Izzr}(N_r, AWG_s, AWG_r) + L'_{Iskr}(N_r, AWG_s, AWG_r)$$

Initial Conditions

$$AWG_{si} := AWG(I_s)$$

$$AWG_{ri} := AWG_{si}$$

$$N_{si} := \frac{Slots_s}{3 \cdot n_s}$$

$$N_{ri} := \frac{Slots_r}{3 \cdot n_r}$$

$$\frac{m}{\omega} := 20$$

$$\frac{\epsilon}{\omega} := .1$$

$$lp := .15$$

```

Design := %i1 ← .1
          AWGsf ← 0
          AWGrf ← 0
          Nsf ← 0
          Nrf ← 0
          AWGs ← AWGsi
          while num_s(AWG_s) > 0
            AWGr ← AWGri
            while wired_AWG_r + 2·width_l < .54·τ_r
              Ns ← Nsi
              while Ns < m·Nsi
                x1 ← 0
                x1 ← 1 if Depth_slot(Ns, AWGs) > .5·tfe
                
$$\Phi_M \leftarrow \frac{E_s \cdot \sqrt{2}}{2 \cdot \pi \cdot f_s \cdot K_s(1, AWG_s) \cdot N_s \cdot \sqrt{3}}$$

                
$$I_s \leftarrow \frac{\sqrt{2} \cdot P_1^2 \cdot g_e(AWG_s, AWG_r) \cdot \Phi_M \cdot \pi}{2 \mu_0 \cdot q \cdot N_s \cdot K_s(1, AWG_s) \cdot D \cdot L_1}$$

                x1 ← 1 if Is > wirea_AWG_s
                x1 ← 1 if Ps > √3·Es·Is
                x1 ← 1 if Ps·(1 + c) < √3·Es·Is
                Nr ← Nri
                while Nr < m·Nri
                  x ← x1
                  x ← 1 if Depth_slot(Nr, AWGr) > .5·tfe
                  
$$E_r \leftarrow \frac{2 \cdot \pi \cdot f_r \cdot K_r(1, AWG_r) \cdot \Phi_M \cdot N_r \cdot \sqrt{3}}{\sqrt{2}}$$

                  x ← 1 if Er > Es
                  
$$I_r \leftarrow \frac{\sqrt{2} \cdot P_1^2 \cdot g_e(AWG_s, AWG_r) \cdot \Phi_M \cdot \pi}{2 \mu_0 \cdot q \cdot N_r \cdot K_r(1, AWG_r) \cdot D \cdot L_1}$$

                  x ← 1 if Ir > wirea_...

```

```

1      AWGr
x ← 1 if .3Ps > √3·E'r·Ir
x ← 1 if .3Ps·(1 + c) < √3·E'r·Ir
x ← 1 if  $\frac{3 \cdot (I_s^2 \cdot R_s(N_s, AWG_s) + I_r^2 \cdot R'_r(N_r, AWG_r))}{\sqrt{3} \cdot E_s \cdot I_s} > \%_1$ 
x ← 1 if  $\frac{L_s(N_s, AWG_s, AWG_r)}{L_{ms}(N_s, AWG_s, AWG_r)} > lp$ 
x ← 1 if  $\frac{L'_r(N_r, AWG_s, AWG_r)}{L'_{mr}(N_r, AWG_s, AWG_r)} > lp$ 
%1 ←  $\frac{3 \cdot (I_s^2 \cdot R_s(N_s, AWG_s) + I_r^2 \cdot R'_r(N_r, AWG_r))}{\sqrt{3} \cdot E_s \cdot I_s}$  if x < 1
AWGsf ← AWGs if x < 1
AWGrf ← AWGr if x < 1
Nsf ← Ns if x < 1
Nrf ← Nr if x < 1
Nr ← Nr + Nri
Ns ← Ns + Nsi
AWGr ← AWGr - 1
AWGs ← AWGs - 1
Design0 ← AWGsf
Design1 ← AWGrf
Design2 ← Nsf
Design3 ← Nrf
return Design
AWGs := Design0      AWGs = 8
AWGr := Design1      AWGr = 2
Ns := Design2        Ns = 608
Nr := Design3        Nr = 380

```

Grid-Connected In-Stream Hydroelectric Generation Based on the Doubly Fed Induction Machine	DFIM Design Sheet	Timothy Lenberg Graduate Student University of Idaho
---	-------------------	--

$$\Phi_M := \frac{\sqrt{2} \cdot E_s}{2 \cdot \pi \cdot f_s \cdot K_s(1, AWG_s) \cdot N_s \cdot \sqrt{3}} \quad \Phi_M = 1.921 \times 10^{-3} \text{ Wb}$$

$$I_{sw} := \frac{\sqrt{2} \cdot P_1^2 \cdot g_e(AWG_s, AWG_r) \cdot \Phi_M \cdot \pi}{2 \mu_0 \cdot q \cdot N_s \cdot K_s(1, AWG_s) \cdot D \cdot L_1} \quad I_s = 12.621 \text{ A}$$

$$\text{wirea}_{AWG_s} = 73 \text{ A}$$

$$E'_r := \frac{2 \cdot \pi \cdot f_r \cdot K_r(1, AWG_r) \cdot \Phi_M \cdot N_r \cdot \sqrt{3}}{\sqrt{2}} \quad E'_r = 94.248 \text{ V}$$

$$I'_r := \frac{\sqrt{2} \cdot P_1^2 \cdot g_e(AWG_s, AWG_r) \cdot \Phi_M \cdot \pi}{2 \mu_0 \cdot q \cdot N_r \cdot K_r(1, AWG_r) \cdot D \cdot L_1} \quad I'_r = 19.284 \text{ A}$$

$$\text{wirea}_{AWG_r} = 181 \text{ A}$$

$$P_{sw} := \sqrt{3} \cdot E_s \cdot I_s \quad P_s = 10.493 \text{ kW}$$

$$P_{ra} := \sqrt{3} \cdot E'_r \cdot I'_r \quad P_r = 3.148 \text{ kW}$$

$$\frac{P_r}{P_s} = 0.3$$

$$P_L := 3 \cdot \left(I_s^2 \cdot R_s(N_s, AWG_s) + I'_r^2 \cdot R'_r(N_r, AWG_r) \right) \quad P_L = 572.355 \text{ W}$$

$$\frac{P_L}{P_s} = 5.455\%$$

$$b_{sws} := b_{os}(AWG_s) \quad b_{os} = 6.647 \text{ mm} \quad \text{Stator Slot Width}$$

$$b_{swr} := b_{or}(AWG_r) \quad b_{or} = 6.624 \text{ mm} \quad \text{Rotor Slot Width}$$

$$t_{sws} := t_{os}(AWG_s) \quad t_{os} = 6.128 \text{ mm} \quad \text{Stator Tooth Width}$$

$$t_{swr} := t_{or}(AWG_r) \quad t_{or} = 6.141 \text{ mm} \quad \text{Rotor Tooth Width}$$

$$T_{sws} := T_s(N_s) \quad T_s = 4 \quad \text{Stator Conductors Per Phase Per Slot}$$

$$T_{swr} := T_r(N_r) \quad T_r = 2.5 \quad \text{Rotor Conductors Per Phase Per Slot}$$

Grid-Connected In-Stream Hydroelectric Generation Based on the Doubly Fed Induction Machine	DFIM Design Sheet	Timothy Lenberg Graduate Student University of Idaho
---	-------------------	--

$$\text{num}_s := \text{num}_s(\text{AWG}_s) \quad \text{num}_s = 2 \quad \text{Number of Conductors Per Stator Slot Width}$$

$$\text{num}_r = 1 \quad \text{Number of Conductors Per Rotor Slot Width}$$

$$\text{Depth}_{\text{sslot}} := \text{Depth}_{\text{sslot}}(N_s, \text{AWG}_s) \quad \text{Depth}_{\text{sslot}} = 13.255 \cdot \text{mm} \quad \text{Stator Slot Depth}$$

$$\text{Depth}_{\text{rslot}} := \text{Depth}_{\text{rslot}}(N_r, \text{AWG}_r) \quad \text{Depth}_{\text{rslot}} = 32.959 \cdot \text{mm} \quad \text{Rotor Slot Depth}$$

$$g_{\text{av}} := g_e(\text{AWG}_s, \text{AWG}_r) \quad g_e = 1.71 \cdot \text{mm}$$

$$N_{\text{se}} := N_{\text{se}}(N_s, \text{AWG}_s) \quad N_{\text{se}} = 689.187$$

$$N_{\text{re}} := N_{\text{re}}(N_r, \text{AWG}_r) \quad N_{\text{re}} = 451.073$$

$$L_{\text{ms}} := L_{\text{ms}}(N_s, \text{AWG}_s, \text{AWG}_r) \quad L_{\text{ms}} = 58.243 \cdot \text{mH}$$

$$L'_{\text{mr}} := L'_{\text{mr}}(N_r, \text{AWG}_s, \text{AWG}_r) \quad L'_{\text{mr}} = 24.95 \cdot \text{mH}$$

$$u := \sqrt{\frac{L_{\text{ms}}}{L'_{\text{mr}}}} \quad u = 1.528$$

$$L_s := L_s(N_s, \text{AWG}_s, \text{AWG}_r) \quad L_s = 7.509 \cdot \text{mH}$$

$$L'_r := L'_r(N_r, \text{AWG}_s, \text{AWG}_r) \quad L'_r = 2.11 \cdot \text{mH}$$

$$L_r := u^2 \cdot L'_r \quad L_r = 4.924 \cdot \text{mH}$$

$$R_s := R_s(N_s, \text{AWG}_s) \quad R_s = 0.877 \Omega$$

$$R'_r := R'_r(N_r, \text{AWG}_r) \quad R'_r = 0.137 \Omega$$

$$R_r := u^2 \cdot R'_r \quad R_r = 0.32 \Omega$$

$$\Omega_s := \frac{\omega_s}{P_1} \quad \omega_s := 2 \cdot \pi \cdot f_s$$

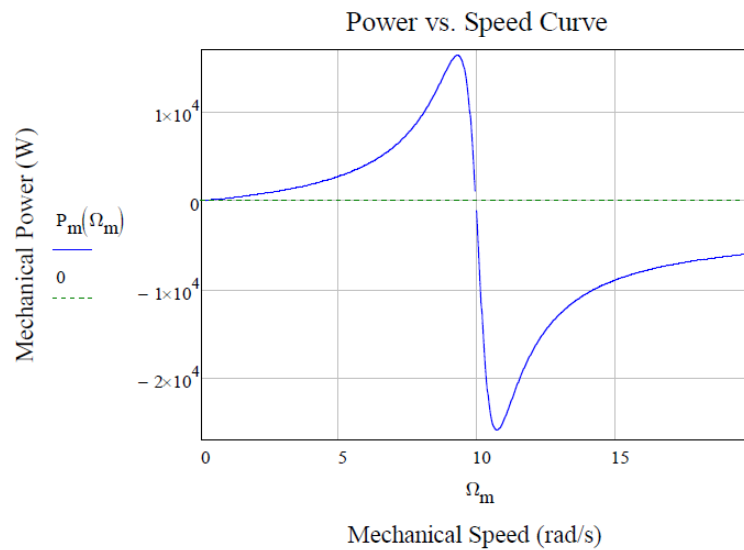
$$s_1(\Omega_m) := \frac{\Omega_s - \Omega_m}{\Omega_s}$$

$$Z_{in}(\Omega_m) := R_s + j \cdot \omega_s \cdot L_s + \left(\frac{1}{\frac{R_r}{s_1(\Omega_m)} + j \cdot \omega_s \cdot L_r} + \frac{1}{j \cdot \omega_s \cdot L_{ms}} \right)^{-1}$$

$$I_s(\Omega_m) := \frac{E_s}{\sqrt{3} \cdot Z_{in}(\Omega_m)}$$

$$I_r(\Omega_m) := \frac{j \cdot \omega_s \cdot L_{ms}}{\frac{R_r}{s_1(\Omega_m)} + j \cdot \omega_s \cdot L_r + j \cdot \omega_s \cdot L_{ms}} \cdot I_s(\Omega_m)$$

$$P_m(\Omega_m) := 3 \cdot (|I_r(\Omega_m)|)^2 \cdot R_r \cdot \frac{(1 - s_1(\Omega_m))}{s_1(\Omega_m)}$$



$$\Omega_m := 10 \frac{\text{rad}}{\text{s}}$$

Given

$$P_m(\Omega_m) = 10 \text{ kW} \quad .9 \cdot \Omega_s < \Omega_m \leq 1.1 \cdot \Omega_s$$

$$\Omega_{\text{mm}} := \text{Find}(\Omega_{\text{m}})$$

$$\Omega_{\text{mm}} = 9.709 \frac{1}{\text{s}}$$

$$\frac{\Omega_{\text{s}} - \Omega_{\text{mm}}}{\Omega_{\text{s}}} = 0.021$$

$$\sqrt{3} \cdot E_{\text{s}} \cdot \overline{I_{\text{s}}(\Omega_{\text{mm}})} = (1.12 \times 10^4 + 1.151i \times 10^4) \text{ W}$$

$$|I_{\text{s}}(\Omega_{\text{mm}})| = 19.322 \text{ A}$$

$$|\sqrt{3} \cdot E_{\text{s}} \cdot \overline{I_{\text{s}}(\Omega_{\text{mm}})}| = 1.606 \times 10^4 \text{ W}$$

Given

$$P_{\text{m}}(\Omega_{\text{m}}) = -10 \text{ kW} \quad .9 \cdot \Omega_{\text{s}} < \Omega_{\text{m}} \leq 1.1 \cdot \Omega_{\text{s}}$$

$$\Omega_{\text{mg}} := \text{Find}(\Omega_{\text{m}})$$

$$\Omega_{\text{mg}} = 10.091 \frac{1}{\text{s}}$$

$$\frac{\Omega_{\text{s}} - \Omega_{\text{mg}}}{\Omega_{\text{s}}} = -0.017$$

$$\sqrt{3} \cdot E_{\text{s}} \cdot \overline{I_{\text{s}}(\Omega_{\text{mg}})} = (-8.954 \times 10^3 + 1.226i \times 10^4) \text{ W}$$

$$|I_{\text{s}}(\Omega_{\text{mg}})| = 18.257 \text{ A}$$

$$|\sqrt{3} \cdot E_{\text{s}} \cdot \overline{I_{\text{s}}(\Omega_{\text{mg}})}| = 1.518 \times 10^4 \text{ W}$$